FWL-TR-75-240

AFWL-TR-
75-240

SATELLITE COMMUNICATIONS IN A SCINTILLATED ENVIRONMENT

Leon A. Wittwer, Captain, USAF

January 1976

Final Report

Approved for public release; distribution unlimited.

AIR FORCE WEAPONS LABORATORY
Air Force Systems Command
Kirtland Air Force Base, NM 87117

This final report was prepared by the Air Force Weapons Laboratory, Kirtland Air Force Base, New Mexico under Job Order 46950113, Captain Wittwer (DYT) was the Laboratory Project Officer-in-Charge.

When US Government drawings, specifications, or other data are used for any purpose other than a definitely related Government procurement operation, the Government thereby incurs no responsibility nor any obligation whatsoever, and the fact that the Government may have formulated, furnished, or in any way supplied the said drawings, specifications, or other data is not to be regarded by implication or otherwise as in any manner licensing the holder or any other person or corporation or conveying any rights or permission to manufacture, use, or sell any patented invention that may in any way be related thereto.

This report has been reviewed by the Information Office (OI) and is releasable to the National Technical Information Service (NTIS). At NTIS, it will be available to the general public including foreign nations.

This technical report has been reviewed and is approved for publication.

Leon A. Wittwer
LEON A. WITTWER
Captain, USAF
Project Officer

FOR THE COMMANDER

Robert G. Surette
ROBERT G. SURETTE
Major, USAF
Deputy Chief, Theoretical Branch

John S. DeWitt
JOHN S. DeWITT
Lt. Colonel, USAF
Chief, Technology Division

DO NOT RETURN THIS COPY. RETAIN OR DESTROY.

UNCLASSIFIED

SECURITY CLASSIFICATION OF THIS PAGE *(When Data Entered)*

REPORT DOCUMENTATION PAGE

READ INSTRUCTIONS BEFORE COMPLETING FORM

1. REPORT NUMBER: AFWL-TR-75-240	2. GOVT ACCESSION NO.
3. RECIPIENT'S CATALOG NUMBER	
4. TITLE *(and Subtitle)*: SATELLITE COMMUNICATIONS IN A SCINTILLATED ENVIRONMENT	5. TYPE OF REPORT & PERIOD COVERED: Final Report
	6. PERFORMING ORG. REPORT NUMBER
7. AUTHOR(s): Leon A. Wittwer, Captain (USAF)	8. CONTRACT OR GRANT NUMBER(s): 62 P.
9. PERFORMING ORGANIZATION NAME AND ADDRESS: Air Force Wapons Laboratory (DYT) Kirtland Air Force Base, NM 87117	10. PROGRAM ELEMENT, PROJECT, TASK AREA & WORK UNIT NUMBERS: 46950113 AT-1695
11. CONTROLLING OFFICE NAME AND ADDRESS: Air Force Weapons Laboratory Air Force Systems Command Kirtland Air Force Base, NM 87117	12. REPORT DATE: January 1976
	13. NUMBER OF PAGES
14. MONITORING AGENCY NAME & ADDRESS *(if different from Controlling Office)*	15. SECURITY CLASS. *(of this report)*: Unclassified
	15a. DECLASSIFICATION DOWNGRADING SCHEDULE

16. DISTRIBUTION STATEMENT *(of this Report)*

Approved for public release; distribution unlimited.

17. DISTRIBUTION STATEMENT *(of the abstract entered in Block 20, if different from Report)*

18. SUPPLEMENTARY NOTES

19. KEY WORDS *(Continue on reverse side if necessary and identify by block number)*

Ionospheric Propagation
Radio Propagation
VHF Propagation
UHF Propagation
Striations
Scintillations

20. ABSTRACT *(Continue on reverse side if necessary and identify by block number)*

An improved method of calculating the statistical properties of a signal propagating through a strongly striated ionosphere is described. Calculations are carried out for a representative equatorial and polar ionosphere. The results are then used to evaluate the performance of an M-ary frequency shift key and a binary phase shift key satellite communications link.

DD FORM 1 JAN 73 1473 EDITION OF 1 NOV 65 IS OBSOLETE

UNCLASSIFIED

SECURITY CLASSIFICATION OF THIS PAGE *(When Data Entered)*

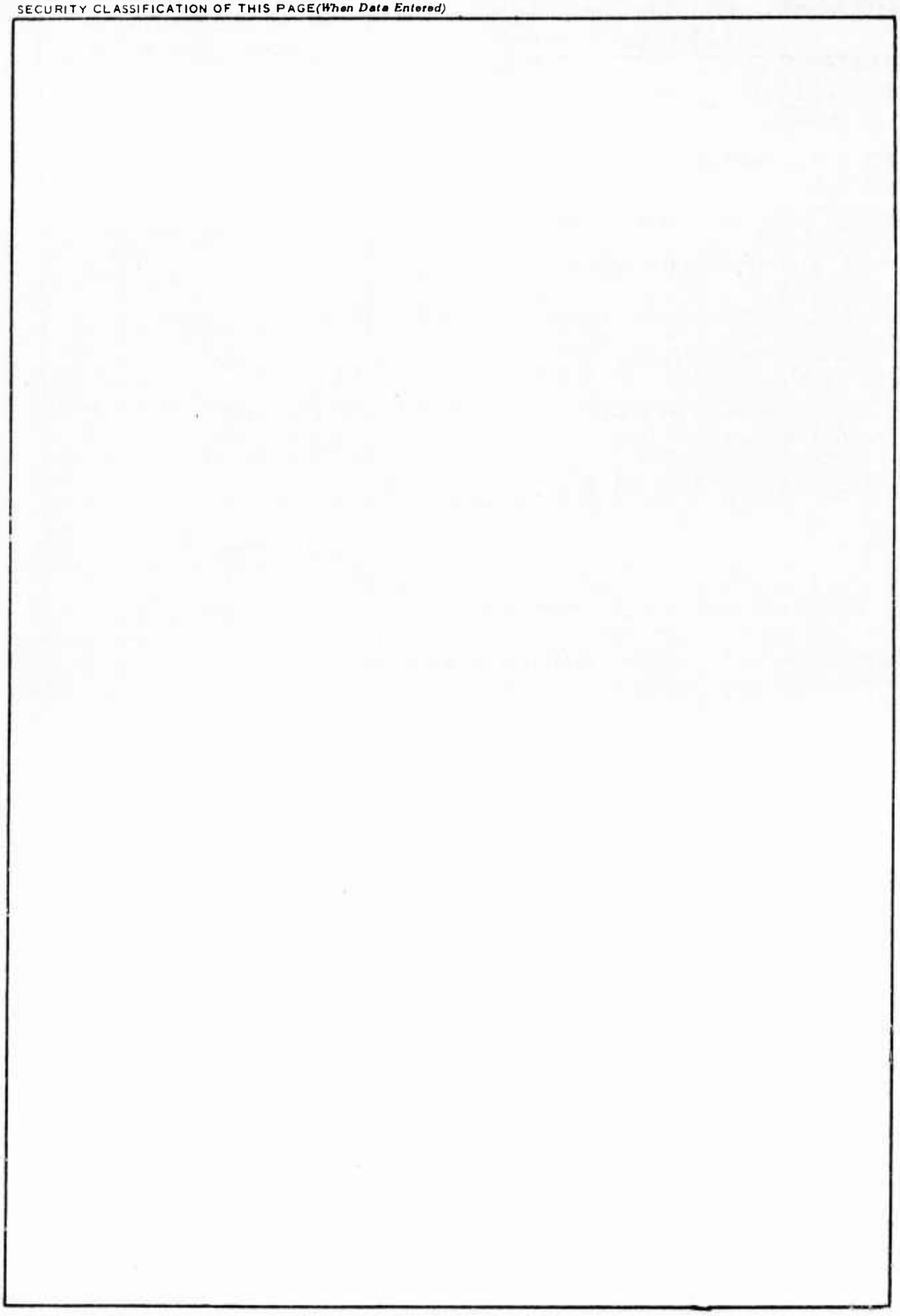

SECTION I

INTRODUCTION

In recent years satellite communications systems have received considerable attention by both commercial and military users. Much of this attention was due to the supposition that the frequency ranges used were insensitive to the ionospheric propagation conditions with the possible exception of absorption from nuclear bursts. This postulated insensitivity made satellite systems very attractive compared to other systems such as HF which rely upon the ionosphere for their operation. The great promise of satellite systems, however, failed to materialize due to the scintillation problem. Scintillations are large fluctuations in the amplitude and phase of a received signal caused by fluctuations in the ionospheric electron density through which the signal passes. An added dimension has been added to the scintillation problem by the realization that similar propagation conditions might result from atmospheric nuclear bursts.

These scintillation problems have created concern on behalf of the military services as satellite communications systems are expected to take an ever increasing roll in military communications. This report is a result of that concern. Contained herein is an analysis of two communication links in two disturbed ambient environments, along with some general discussion of ionospheric environments.

The two systems treated are an M-ary frequency shift key system (MFSK) and a binary phase shift system (BFSK). It is hoped that the discussion and calculation results will be useful to others working in this area as well as better defining the scintillation difficulties encountered by these systems.

This document consists of seven sections excluding the introduction. The second section discusses the propagation methods used and their justification. The third and fourth sections discuss the frequency shift key and the binary phase shift key models, respectively. The determination and a discourse on the environments used are found in the fifth section. Next the results of some calculations are presented. A brief summary concludes this paper.

SECTION II

PROPAGATION

With the advent of satellite communication links and the discovery of scintillated signal conditions under the equatorial and polar ionospheres, it has become necessary to extend VHF, UHF, and higher frequency propagation techniques (ref 1 to 8). These methods were generally based on a thin screen approximation geometrical optics, weak scattering, or some combination of these approximations. The method presented here is not restricted by the above approximations and also, for many situations, supplies more information on the statistical properties of the propagated wave than do the previous methods.

There is, already in existence, a method by Uscinski (ref 9) is not subject to the above limitations. This previous method will calculate the same information as the method presented here, but appears more difficult numerically to evaluate.

Let the signal incident on the ionosphere be represented as

$$E = (\overline{E} + E_R + i\, E_I)e^{iKX} \qquad (1)$$

where

$\overline{E}$ = mean field

E_R = in phase quadrature component

E_I = out of phase quadrature component

$K = 2\pi/\lambda$

Let me define two statistical quantities called the complex autocorrelation

function and the asymmetry autocorrelation function, respectively, where an overline, $\overline{\quad}$, represents the ensemble average:

$$G(X,\rho) = \overline{E^*(X,Z)\ E(X,Z+\rho)}$$

$$= \overline{E}^2 + \overline{E_R(X,Z)E_R(X,Z+\rho)} + \overline{E_I(X,Z)E_I(X,Z+\rho)} \qquad (2)$$

$$F(X,\rho) = \overline{E(X,Z)E(X,Z+\rho)}$$

$$= \overline{E}^2 + \overline{E_R(X,Z)E_R(X,Z+\rho)} - \overline{E_I(X,Z)E_I(X,Z+\rho)}$$

$$+ 2i\ \overline{E_R(X,Z)E_I(X,Z+\rho)} \qquad (3)$$

since $\overline{E_R(X,Z)} = \overline{E_I(X,Z)} = 0$ and $\overline{E_R(X,Z)E_I(X,Z+\rho)} = \overline{E_I(X,Z)E_R(X,Z+\rho)}$.

The symmetry in the cross correlation of E_R and E_I will result from certain assumptions about the striated medium. The second transverse coordinate will be suppressed for convenience. Its inclusion in the expressions that follow is a minor matter.

Tatarskii (ref 10) explicitly derived th equations for the mean field and the complex autocorrelation function. The equation for the asymmetry autocorrelation function can be derived similarly to the complex autocorrelation function. The equations are

$$\frac{d\overline{E}(X)}{dX} = -K^2\overline{E}(X)A(X,0)/2 \qquad (4)$$

$$\frac{dF(X,\rho)}{dX} = \frac{i}{K}\frac{d^2F(X,\rho)}{d\rho^2} - K^2F(X,\rho)[A(X,0) + A(X,\rho)] \qquad (5)$$

$$\frac{dG(X,\rho)}{dX} = -K^2\ G(X,\rho)[A(X,0) - A(X,\rho)] \qquad (6)$$

where

$$A(X,\rho) = \int_{-\infty}^{\infty} \overline{n(X,Z)n(X',Z+\rho)}\, dX'$$

n(X,Z) = index of refraction fluctuations

"n(X,Z)" is assumed to be a zero mean gaussian random variable. These conditions on n(X,Z) are sufficient but not in all cases necessary to the derivation of equations 5 and 6. For example, if a signal suffers many scatters traversing a striated medium, then equations 5 and 6 can be justified by using the central limit theorem. In any event experimental work at SRI[2] has shown the assumption of Gaussian distributed fluctuations to be justified. Equation 4 is not necessary as $G(X,\infty) \bullet \overline{E(X)}^2$, but it is carried in calculations to examine the degree to which the boundary conditions on $F(X,\rho)$ and $G(X,\rho)$ are satisfied.

The limitations on the solutions of equations 5, 6, and 7 are discussed in Tatarskii (ref 10) and will be summarized here.

$$\lambda << \ell_o \tag{8}$$

$$L >> \ell_o \tag{9}$$

$$\lambda\ \alpha << 1 \tag{10}$$

$$\sigma_\theta^2 << 1 \tag{11}$$

$$\alpha L \sigma_\theta^2 << 1 \tag{12}$$

$$L << X_m \tag{13}$$

where

ℓ_o = striation scale size

L = striation layer thickness

α = mean field attenuation coefficient

σ_θ^2 = mean square scattering angle

X_m = characteristic distance for attenuation by back scattering

All of these conditions are easily met for present problems of interest. An implicit assumption in using the $A(X,\rho)$ function with an explicit X dependence, is that the variation of A along X is small over a scale size. If the striated medium is homogeneous, then $A(X,\rho)$ is symmetric with respect to ρ. The symmetry in ρ results in like symmetry in $F(X,\rho)$ and $G(X,\rho)$.

The functions $F(X,\rho)$ and $G(X,\rho)$ are not the most useful qualities. Instead, the correlation functions of the field components are the ultimate product.

$$\overline{E_R(X,Z)E_R(X,Z+\rho)} = [G(X,\rho) + \text{Real}(F(X,\rho))]/2 - \bar{E}^2 \tag{14}$$

$$\overline{E_I(X,Z)E_I(X,Z+\rho)} = [G(X,\rho) - \text{Real}(F(X,\rho))]/2 \tag{15}$$

$$\overline{E_R(X,Z)E_I(X,Z+\rho)} = \text{Imag}(F(X,\rho))/2 \tag{16}$$

The correlation function of the index of refraction fluctuations used in all present calculations is of the form

$$\overline{n(X,Y,Z)n\ (X+\varepsilon,\ Y+\rho,\ Z+\eta)} = \tag{17}$$

$$C(\omega)\ \overline{n_e(X)}^2\ \delta n^2\ \exp\ \left[-(\varepsilon^2+\rho^2+\eta^2)^{1/2}/\ell_o\right]$$

where $$C(w) = \left(\frac{2\pi e^2}{m\omega^2}\right)$$

$\overline{n_e(X)}$ = mean electron density

ℓ_o = outer scale size

δ_n^2 = local value of $(\overline{n_e^2} - \overline{n_e}^2)/\overline{n_e}^2$

The one sided power spectral density (PSD) of the electron density fluctuations corresponding to equation 17 is

$$PSD(K) = \frac{\overline{n_e(X)}^2 \, \delta_n^2 \, \ell_o^3}{2\pi^2(1 + K^2\ell_o^2)^2} \tag{18}$$

In actual ionospheric experiments the electron density fluctuations are measured along a given path. The one-dimensional form of (18) is

$$PSD(K_\perp) = \frac{\overline{n_e(X)}^2 \, \delta_n^2/\ell_o}{\pi(1/\ell_o^2 + K_\perp^2)} \tag{19}$$

where $K_\perp$ is perpendicular to the local magnetic field and K parallel is assumed to be zero. This last assumption is often very reasonable as the ionospheric structure tends to elongate along the ambient magnetic field. This form of the PSD closely fits data measured by several authors (ref 11 *). The correlation function assuming the propagation path is perpendicular to the magnetic field is reduced to

$$\overline{n(X,Y)\; n(X + \varepsilon, Y + \rho)} = C(\omega) \; \overline{n_e(X)}^2 \; \delta_n^2 \; \exp\left[-(\varepsilon^2 + \rho^2)^{1/2}/\ell_o\right]. \tag{20}$$

*Private communication with M.C. Kelley and K.C. Yeh.

This form is used in equation 7 for propagation calculations near the equator. When propagation in some polar scenarios is calculated, the lines of sight are sometimes more parallel than perpendicular to the field lines. In this case equation 17 is used with $\chi^2 = \rho^2 + \eta^2$, and the transverse operator in equation 5 is replaced as follows

$$\frac{d^2}{d\rho^2} = \frac{d^2}{d\chi^2} + \frac{1}{\chi}\frac{d}{d\chi} \tag{21}$$

In the analysis of the communication links to follow, it is assumed that E_R and E_I are Gaussian random variables. This assumption is reasonable when the propagation disturbance is small since the propagation is still linear and Gaussian distributed electron density fluctuations were assumed. The Gaussian assumption also is valid for the strong multiscatter case as the resultant propagated signal is the sum of many independent scattered signals. In between these two extremes, the matter is not so clear.

Fortunately the fourth order moments of the propagated signals for some ionospheric cases have been calculated by Yeh*. The root mean square of the amplitude fluctuations was deemed to be the most useful measure of the Gaussian assumption. The maximum error in the mean square amplitude fluctuation between 100 and 1000 MHz was about 18 percent with the value using the Gaussian assumption being the largest. Fremouw and Rhino (ref 12) have also shown that scintillation data are consistent with the Gaussian assumption.

It is important to remember at this point that the propagation does calculate the first and second moments of the field correctly, and the

---

* Private communication with K.C. Yeh.

gaussian assumption on E_R and E_I is an added feature independent of the propagation.

All of the propagation discussion thus far has dealt with the propagation of a single frequency. With the consideration of spread spectrum techniques, it is necessary to know the correlation of signals of different frequencies to evaluate these techniques. The equation to calculate two frequency correlations is a generalization of equation 6 and was first used extensively by Liu (ref 13) and Ulaszek (ref 14).

$$\frac{dH(X,\rho)}{dX} = \frac{i(K_1-K_2)}{2K_1K_2}\frac{d^2H(X,\rho)}{d\rho^2} - \frac{K_\rho}{4K_1K_2}\left(\frac{(K_1^2+K_2^2)}{2K_1K_2}\ A_n(X,0) - A_n(X,\rho)\right) H(X,\rho) = 0 \tag{22}$$

where

$$H(X,\rho) = \overline{E_{K_1}^{*}(X,Z)\ E_{K_2}(X,Z+\rho)}$$

$$A_n(X,\rho) = \int_{-\infty}^{\infty} \overline{\Delta n_e(X,Z)\Delta n_e(X+\eta, Z+\rho)}\ d\eta$$

$\Delta n_e(X,Z)$ = electron density fluctuations

$$K_\rho^2 = \frac{4\pi e^2}{mc^2}$$

The real part of $H(X,0)$ is taken as the correlation coefficient where initially

$$\overline{E_{K_1}^{*}(0,Z)\ E_{K_2}(0,\ Z+\rho)} = 1. \tag{23}$$

The imaginary part is the sine of the phase difference between the two frequencies not including dispersion.

In real practical problems the electromagnetic waves are not plane

waves but have some curvature. Because of this, it is necessary to examine the limits of the plane wave formalism. The following will be done in two dimensions to illustrate the desired limits. The general form of a cylindrical wave is

$$E = \mu_o(X,\rho) \frac{e^{i K(X^2+\rho^2)^{1/2}}}{(X^2+\rho^2)^{1/4}} \tag{24}$$

where in the absence of propagation effects

$$\mu_o(X,\rho) = 1 \tag{25}$$

Equation 14 can be expanded

$$E \approx \mu_o(X,\rho) \frac{e^{i \frac{K\rho^2}{2X}}}{X^{1/2}} \ell^{iKX} \equiv \mu(X,\rho) e^{iKX} \tag{26}$$

For $\rho \leq 7$ km and X = 250 km, the amplitude of the approximation is in error about 5 percent. For any frequency and the same ρ and X, the radius of the wave front is off by ≤ 4 cm. This error is insignificant for present purposes, even though this may be several radians in phase at higher frequencies. This is because we are interested in the incoherent scattering of energy where kilometers of propagation path are needed to see any effects. The complex correlation function is

$$\overline{\mu^*(X,\rho_2)\mu(X,\rho_1)} = \overline{\mu_o^*(X,\rho_2)\mu_o(X,\rho_1)} \frac{e^{i \frac{K}{2X}(\rho_1^2 - \rho_2^2)}}{X} \tag{27}$$

If $Z = \rho_1 - \rho_2$ and $R = \frac{1}{2}(\rho_1 + \rho_2)$, $\overline{\mu^*(X,\rho_2)\mu(X,\rho_1)} = G(X,R,Z)$, and

$$\mu_o^*(X,\rho_2)\mu_o(X,\rho_1) = G_o(X,R,Z), \text{ then } G(X,R,Z) = G_o(X,R,Z)\frac{e^{i\frac{KRZ}{X}}}{X} \tag{28}$$

From Tatarskii (ref 10), the equation for G(X,R,Z) is

$$\frac{\partial G(X,R,Z)}{\partial X} - \frac{i}{K}\frac{\partial}{\partial Z}\frac{\partial}{\partial R}G(X,R,Z) + K^2\,[A(X,0) - A(X,Z)]\,G(X,R,Z) = 0 \tag{29}$$

In the limit of a plane wave $\frac{\partial G(X,R,Z)}{\partial R} = 0$, and equation 6 is obtained.

For initial conditions on G(X,R,Z), $G_o(X,R,Z)$ is set to one. It is easy to show that if there is no scattering, that is, A(X,Z) = 0, then equation 28 is a solution of equation 29. This results because equation 26 is an exact solution to the parabolic equation.

Substituting equation 28 into equation 29,

$$\frac{dG_o(X,R,Z)}{dX} - \frac{i}{K}\left[\frac{\partial^2 G_o(X,R,Z)}{\partial Z \partial R} + \frac{iK}{X}\left(R\frac{\partial}{\partial R}G_o(X,R,Z) + Z\frac{\partial G_o(X,R,Z)}{\partial Z}\right)\right] + K^2[A(X,0) - A(X,Z)]\,G_o(X,R,Z) = 0 \tag{30}$$

Since the initial condition on G_o has no R dependence, it can never develop any. Thus

$$\frac{dG_o(X,R,Z)}{dX} + \frac{Z}{X}\frac{\partial G_o(X,R,Z)}{\partial Z} + K^2\,[A(X,0) - A(X,Z)]\,G_o(X,R,Z) = 0 \tag{31}$$

$G_o(X,R,Z)$ at large Z is the fraction of power not scattered and is identical with the plane wave result. The second term in equation 31 is a geometrical divergence term. Thus the solution to equation 31 looks approximately like the plane wave solution with the transverse coordinate scaled as $\frac{X_o}{X}$ where X_o is the center of the scattering layer.

The asymmetry auto-correlation function is

$$\overline{\mu(X,\rho_2)\mu(X,\rho_1)} = \overline{\mu_o(X,\rho_2)\mu_o(X,\rho_1)} \quad \frac{e^{i\frac{K}{2X}(\rho_1^2+\rho_2^2)}}{X} \tag{32}$$

Thus, as before,

$$F(X,R,Z) = F_o(X,R,Z) \frac{e^{i\frac{K}{2X}(2R^2+Z^2/2)}}{X} \tag{33}$$

The equation for F(X,R,Z) is

$$\frac{\partial F(X,R,Z)}{\partial X} + \frac{1}{2iK}\left[2\frac{\partial^2}{\partial Z^2} + \frac{1}{2}\frac{\partial^2}{\partial R^2}\right]F(X,R,Z)$$

$$+ K^2\,[A(X,0) + A(X,Z)]F(X,R,Z) = 0 \tag{34}$$

As before if $A(X,Z) = 0$, then $F(X,R,Z)$ is an exact solution to equation 34 with $F_o(X,R,Z) = 1$ as the boundary condition. The equation for $F_o(X,R,Z)$ is

$$\frac{\partial F_o(X,R,Z)}{\partial X} - \frac{i}{K}\frac{\partial^2 F_o(X,R,Z)}{\partial Z^2} + \frac{Z}{X}\frac{\partial F_o(X,R,Z)}{\partial Z}$$

$$+ K^2[A(X,0) + A(X,Z)]F_o(X,R,Z) = 0 \tag{35}$$

$F_o(X,R,Z)$ is not a function of R since $A(X,Z)$ is not. Again, there is the plane wave equation plus a geometric divergence term. As in the complex autocorrelation function, $F_o(X,R,Z)$ looks very much like the plane wave solution with the transverse coordinate scaled as X_o/X. Thus the pictures for $F_o(X,R,Z)$ and $G_o(X,R,Z)$ are the same.

For spherical waves with an axisymmetric electron fluctuation correlation function, equations 31 and 35 remain the same except that $\frac{\partial^2}{\partial Z^2}$ goes to $\frac{\partial^2}{\partial Z^2} + \frac{1}{Z}\frac{\partial}{\partial Z}$ and that R and Z are now radial coordinates. To visualize the final physical result, imagine the solutions to equations 31 and 35 being wrapped along the curved wave surface. This wrapping is accomplished mathematically by the phase terms in equations 28 and 33

The conclusion of this analysis is that the plane wave results with X_o/X scaling varies little from the cylindrical and spherical wave results. Calculations verify this result.

In summary adequate methods exist to calculate the propagation effects of a turbulent ionosphere on traversing signals. The included equations allow the calculation of the first and second order signal statistics at one frequency as well as two frequency statistics. Fourth order moments of the signal are calculable as in the calculations of Yeh*. In general, however, the calculation of the fourth moments are very expensive; thus the use of the Gaussian assumption on the quadrature components of the signals.

The calculation methods described here are relatively inexpensive. In general less than 3 minutes of CPU time on a CDC 6600 were needed per calculation for either plane, cylindrical, or spherical geometries.

---

*Private communication with K.C. Yeh.

M-ARY FREQUENCY SHIFT KEY DEMODULATOR

The received signal is assumed to be of the form

$$S_n(t) = [\bar{E} + E_R(t) + iE_I(t)]e^{i2\pi(f_c + n\frac{\Delta f}{2} + f_o)t} + N(t) \qquad (36)$$

where $\bar{E}$ = mean field

$E_R(t)$ = in-phase component

$E_I(t)$ = out-of-phase component

f_c = carrier frequency

Δf = frequency shift

f_o = carrier frequency error

n = frequency shift number

$N(t)$ = white gaussian noise

For a binary system n equals ± 1, and for an 8-ary system n equals ± 1, ± 3, ± 5 and ± 7. The in-phase and out-of-phase components are assumed random Gaussian variables.

The demodulator is a group of matched filter-rectifier pairs in parallel. Figure 1 contains a binary system. The operation of the matched filter matched to the incoming signal is

$$R_n = \frac{E_o}{N}\int_0^T S(t)\, \ell^{-i\,2\pi(f_c + \frac{n\,\Delta f}{2})t}\, dt \qquad (37)$$

where R_n = dumped filter output at T

N = unilateral noise power spectral density

E_o = expected signal strength

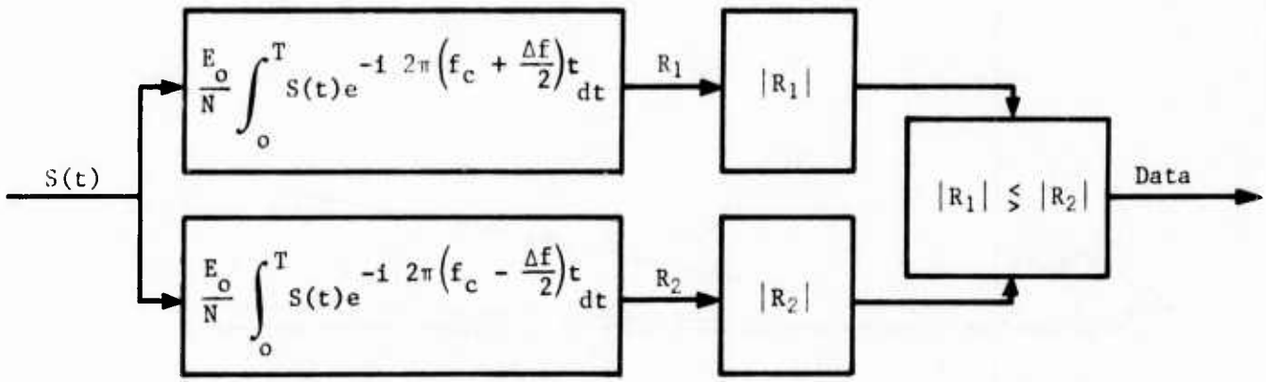

Figure 1 Binary FSK demodular

The operation of the rectifier following the matched filter is represented by taking the absolute value of R_n. The output of the m filter, assuming the n signal is being transmitted, is

$$R_m = \frac{E_o}{N}\int_o^T \left[\bar{E} + E_R(t) + iE_I(t)\right] e^{i\,2\pi\left((n-m)\frac{\Delta f}{2}+f_o\right)t} dt$$

$$+ \frac{E_o}{N}\int_0^T N(t)e^{-i\,2\pi\left(f_c+m\frac{\Delta f}{2}\right)t} dt \qquad (38)$$

The outputs of the filters consist of the sum of two complex numbers. The first is a deterministic term dependent on the received signal, the particular filter, and the total phase error. The second term is the random noise term. Figure 2 portrays an example of the output of the filters of a binary system with n equal 1. The vectors from the origin, $\bar{r}_1$ and $\bar{r}_2$, represent the deterministic terms, and the second vectors are the noise terms.

From the previous discussion it is clear that the noise vector is random in orientation with a Rayleigh distributed amplitude. Given

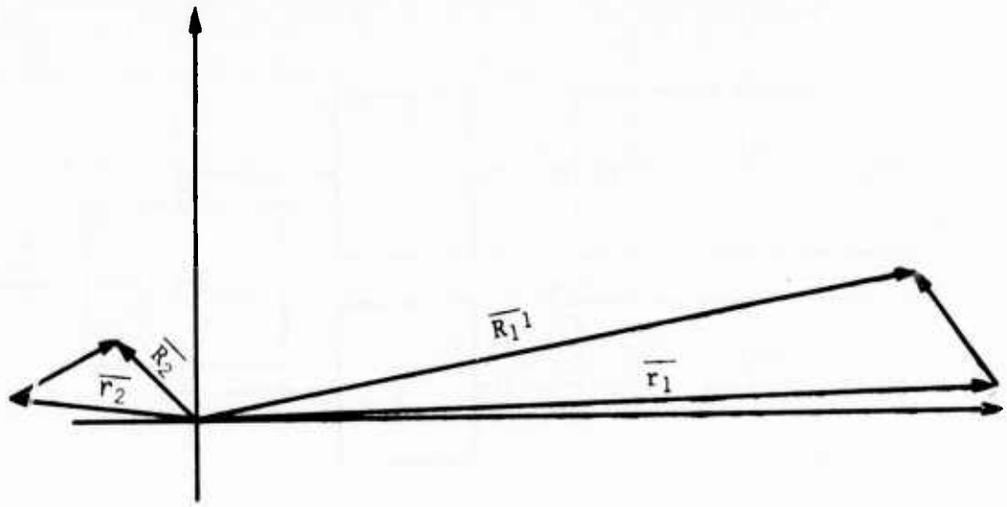

Figure 2. Sample Filter Output

$\bar{r}_1$, $\bar{r}_2$, and knowing the noise statistics the probability of error, i.e., $|\bar{R}_2| > |\bar{R}_1|$, can be calculated (ref 15). Let

$$d^2 = \frac{E_o{}^2 T}{N} \tag{39}$$

$$\alpha = \frac{|\bar{r}_1|}{\sqrt{2}\, d} \tag{40}$$

$$\beta = \frac{|\bar{r}_2|}{\sqrt{2}\, d} \tag{41}$$

Then the probability of error is

$$P_e = 1 - Q(\alpha,\beta) + \frac{1}{2} e^{-\frac{(\alpha^2+\beta^2)}{2}} I_o(\alpha\beta) \tag{42}$$

$$1-Q(\alpha,\beta) = e^{\frac{-(\alpha^2+\beta^2)}{2}} \left[\frac{\beta}{\alpha} I_1(\alpha\beta) + \left(\frac{\beta}{\alpha}\right)^2 I_2(\alpha\beta) + \ldots \right] \tag{43}$$

"d^2" is the signal to noise ratio. It is also twice the baud energy-to-noise ratio. $I_n(X)$ is the conventional integer order modified Bessel function.

The simulation of an M-ary system proceeds as follows. First using the method described in appendix A, a random sample of $\bar{E} + E_R(t) + iE_I(t)$ is generated. Given f_o and n designating the signal present, R_m is determined at appropriate sampling times. For each sampling time the probability of error is one minus the product over $m \neq n$ of the probabilities that $|R_m| < |R_n|$. This probability of error at each sampling time is then used to determine various performance parameters of the system. The channel containing the signal is chosen randomly. Meaningful statistics are achieved by processing a sufficient number of sample signals.

This methodology allows simulation of all the major aspects of this type of receiver. In particular nonorthogonality of channels and frequence error in the incoming carrier are included. The simulations are inexpensive, consuming less than 3 minutes of CPU times on a CDC 6600.

SECTION IV

BINARY PHASE SHIFT KEY DEMODULATOR

The received signal is represented as

$$E'(t) = M(t)\ [\bar{E} + E_R(t) + i\ E_I(t)]\ e^{i\ 2\pi f_c t} \tag{44}$$

where

$\bar{E}$ = mean field

$E_R(t)$ = in phase component

$E_I(t)$ = out of phase component

f_c = carrier frequency

$M(t)$ = modulation

$M(t)$ is either ± 1 during each bit period corresponding to a 0 or a 1 bit. For purposes of analysis only, the real part of equation 44 is necessary. $E_R(t)$ and $E_I(t)$ are assumed Gaussian distributed. Let

$$s(t) = \text{Real}\ [E'(t)] \tag{45}$$

$$= M(t)\ E(t)\ \cos\ (\theta(t) + 2\pi f_c t) \tag{46}$$

where

$$E(t) = [(\bar{E} + E_R(t))^2 + E_I{}^2(t)]^{1/2}$$

$$\theta(t) = \tan^{-1}[E_I(t)/(\bar{E} + E_R(t))]$$

The model demodulator is described in figure 3.

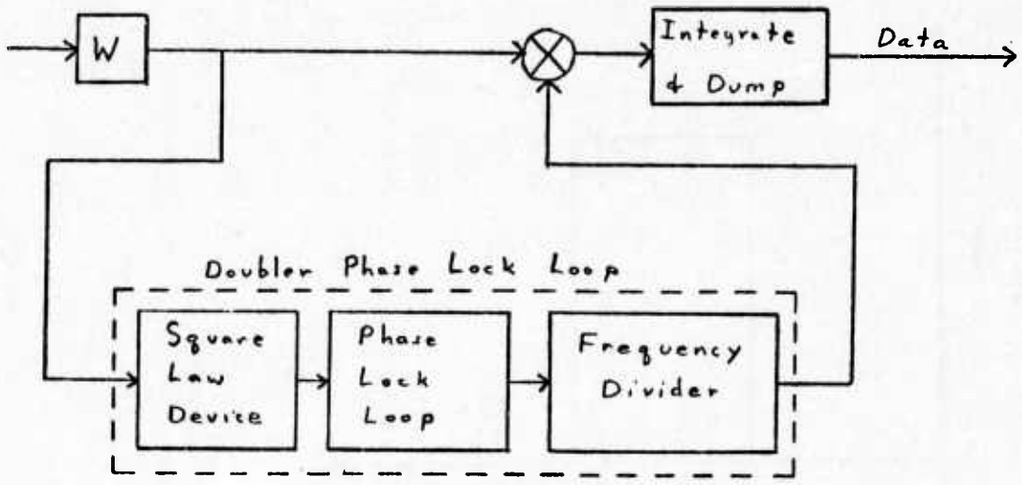

Figure 3. Demodulator Model

The incoming signal is first filtered by an IF filter with a one sided bandwidth of W. The signal then goes to a multiplier and a doubler phase-locked-loop (DPLL). The DPLL generates a coherent reference which is fed into the multiplier and is multiplied by the original signal. The multiplier result is integrated over a baud period and the data determined. This is essentially the same model as in reference 9.

The demodulator description will consist of two sections. The first will discuss the IF filter and the doubler phase-locked-loop. The second will treat the multiplier and the integrator. The initial discussion to follow parallels closely the discussion in reference 9.

IF Filter and DPLL

The IF filter is assumed to have the following transfer function.

$$H(f) = \pi\left(\frac{f-f_o}{W}\right) + \pi\left(\frac{f+f_o}{W}\right) \qquad (47)$$

where f_o is the carrier frequency and $\pi\left(\frac{x-y}{z}\right)$ is shown in figure 4.

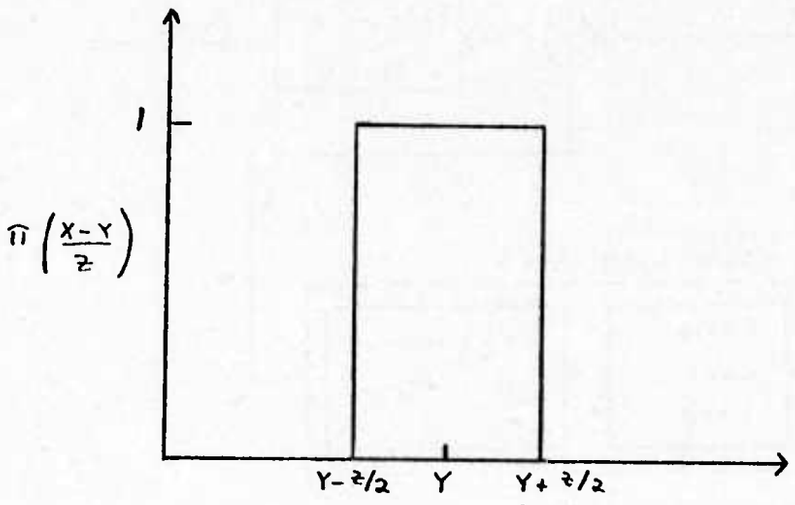

Figure 4. π Function

The input noise spectrum is assumed constant over the bandwidth of the filter thus the power spectral density of the filtered noise is

$$S_n(f) = \frac{N_o}{2}\left[\pi\left(\frac{f-f_o}{W}\right) + \pi\left(\frac{f+f_o}{W}\right)\right] \tag{48}$$

where N_o is the unilateral spectral density of the noise

The first element in the DPLL is a square law device. This device removes the BPSK modulation. With an input signal of

$$v(t) = s(t) + n(t) \tag{49}$$

$$s(t) = M(t)\ E(t)\ \cos\ (\theta(t) + 2\pi\ f_o t) \tag{50}$$

the output is

$$s^2(t) = \frac{E^2(t)}{2} \left[1 + \cos\left(4\pi f_o t + 2\theta(t)\right)\right]$$

$$+ 2M(t)\, E(t) \cos\left(2\pi f_o t + \theta(t)\right) n(t) + n^2(t) \qquad (51)$$

The last two terms in equation 51 are noise derived terms. The power spectral density of these terms is derived in appendix B.

$$S_n{}^2(f) = 4S_n(f) * S_s(f) + 2S_n(f) * S_n(f)$$

$$+ \text{DC terms} \qquad (52)$$

where $S_s(f)$ is the power spectral density of the signal, s(t). The $S_n(f) * S_n(f)$ term is readily evaluated.

$$2S_n(f) * S_n(f) = \frac{N_o{}^2 W}{2} \left[\Lambda\left(\frac{f-2f_o}{2W}\right) \right.$$

$$\left. + \Lambda\left(\frac{f+2f_o}{2W}\right) + 2\Lambda\left(\frac{f}{W}\right) \right] \qquad (53)$$

where the Λ function is illustrated in figure 5.

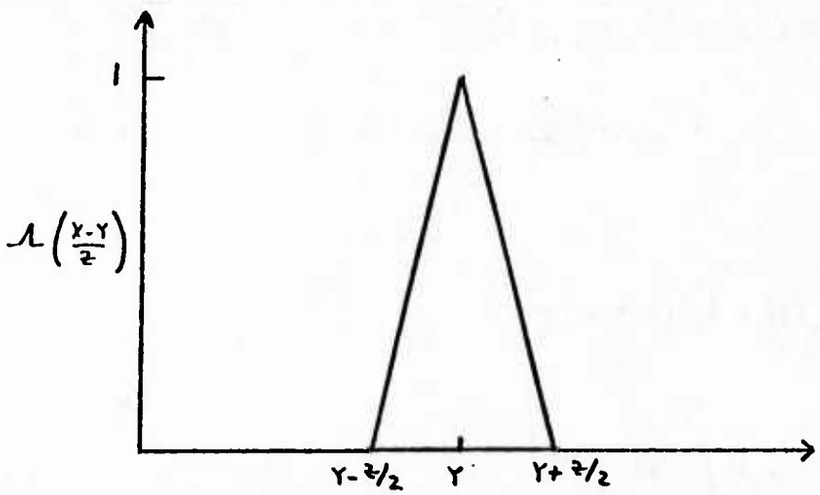

Figure 5. Λ Function

Let us now look at the $S_n \times S_s$ term where

$$s(t) = M(t)\, E(t) \cos\,(2\pi f_o t + \theta(t)) \tag{54}$$

If E(t) and $\theta(t)$ are assumed to change slowly with respect to the carrier frequency, then $S_s(f)$ can be written as

$$S_s(f) = \frac{1}{4}\,[S_b(f-f_o) + S_b(-f-f_o)] \tag{55}$$

where

$$S_b(f) = \pi\left(\frac{f}{W}\right) S_c(f) \tag{56}$$

and $S_c(f)$ is the power spectral density of $M(t)E(t)e^{i\theta(t)}$. As W decreases some of the signal power is lost. Let the fraction of signal power that is lost be N_f. Then

$$\int_{-\infty}^{\infty} S_b(f)df = N_f \int_{-\infty}^{\infty} S_c(f)df \tag{57}$$

where $\int_{-\infty}^{\infty} S_c(f)df$ is twice the received signal power.

From equations 48 and 55 the $S_n \times S_s$ term can be evaluated.

$$S_s(f) * S_n(f) = \frac{No}{8}\,[S_{bn}(f+2f_o) + S_{bn}(f-2f_o) + 2S_{bn}(f)] \tag{58}$$

where

$$S_{bn}(f) = S_b(f) * \pi\left(\frac{f}{W}\right) = \int_{-W/2}^{W/2} S_b(f-\mu)\,d\mu \tag{59}$$

From equations 53 and 58 the total power spectral density of the noise out of the square law device is

$$S_n^2(f) = \frac{N_o}{2} [S_{bn}(f+2f_o) + S_{bn}(f-2fo)] + \frac{No^2W}{2} \left[\Lambda\left(\frac{f-2f_o}{W}\right) + \Lambda\left(\frac{f-2f_o}{W}\right)\right] + \text{low frequency terms} \quad (60)$$

The total noise power out of the square law device in the side bands is

$$\int_{-\infty}^{\infty} S_n 2(f)df = 2N_o^2W^2 + 2N_oWQ(t)N_f \quad (61)$$

where Q(t) is the received signal power. The time dependence in Q(t) denotes the variation of signal power from scintillations, absorption, and such effects. In terms of E(t)

$$Q(t) \approx E^2(t)/2 \quad (62)$$

In the discussion of the phase lock loop (PLL) to follow, it will be noted that only the input frequencies in a narrow band B_L centered about $\pm 2f_o$ are important. B_L is called the loop bandwidth. Since B_L is usually much smaller than W, the noise output out of the square law device is characterized as gaussian with a unilateral power spectral density of

$$N = 2N_o Q(t)\ N_s + N_o^2W \quad (63)$$

The $S_n \times S_n$ noise output is not actually gaussian but has a χ^2 distribution. If $B_L < W$, however, the term can be considered gaussian since the PLL operation is equivalent to an integration over many decorrelation times of the noise input. The output signal of the square law device is now represented as

$$S^2(t) = \sqrt{2P(t)}\ \sin\ (2\pi f_c t + \phi(t)) + n'(t) \tag{64}$$

where $P(t) = E^4(t)/8$

$f_c = 2f_o$

$\phi(t) = 2\theta(t) - \pi/2$

$n'(t)$ = noise characterized by equations 60 and 63

The change in symbols is to conform to the discussion in reference 20 where the phase lock loops of present concern are described in greater detail. Figure 6 is a diagram of the phase lock loop to be modeled.

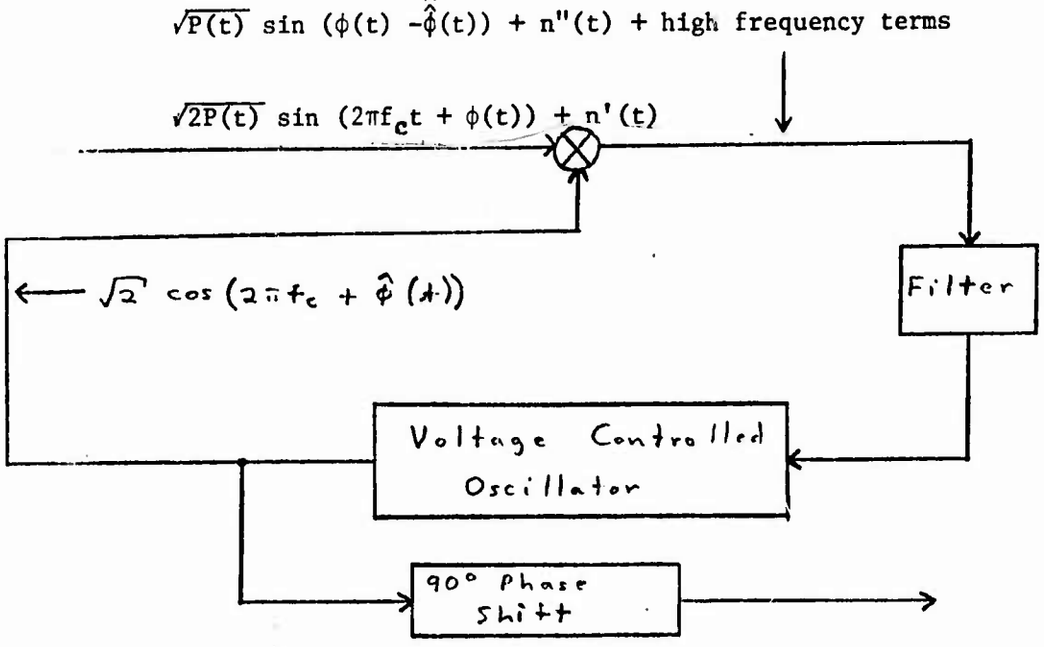

Figure 6. Phase Lock Loop

n"(t) is a zero mean Gaussian process with bandwidth W, spectral height N/2, and center frequency zero. In figure 6, $\hat{\phi}(t)$ is the phase estimate of the incoming signal. The high frequency terms out of the multiplier will be filtered out so they will be dropped. The output of the voltage controlled oscillator (VCO) is a sinusoid with a frequency shift proportional to the input. The output is written as

$$\sqrt{2}\cos\left(2\pi f_c t + a\int^{t} f(u)\,du\right)$$

$$= \sqrt{2}\cos\left(2\pi f_c t + \hat{\phi}(t)\right) \tag{65}$$

where f(u) is the input to the VCO. "a" will be taken as equal to one.

Two filters will be considered. The first is just a gain, $K/\sqrt{P_o}$, where P_o is the value of P(t) with no propagation effects. The analysis of this first order loop is straightforward

$$f(t) = K\sqrt{\frac{P(t)}{P_o}}\sin\left[\phi(t) - \hat{\phi}(t)\right] + \frac{K}{\sqrt{P_o}}\,n''(t)$$

$$= \frac{d\hat{\phi}(t)}{dt} \tag{66}$$

Let $e(t) = \phi(t) - \hat{\phi}(t)$

Then $$\frac{de(t)}{dt} = -K\sqrt{\frac{P(t)}{P_o}}\sin\left[e(t)\right] - \frac{K}{\sqrt{P_o}}\,n''(t) + \frac{d\phi(t)}{dt} \tag{67}$$

The second filter has a response of $\frac{K}{\sqrt{P_o}}\left(1 + \frac{a}{s}\right)$. Thus

$$\frac{de(t)}{dt} = -K \sqrt{\frac{P(t)}{P_o}} \sin (e(t)) - \frac{K}{\sqrt{P_o}} n''(t)$$

$$- a_1 K \int_o^t \left[\sqrt{\frac{P(u)}{P_o}} \sin (e(u)) + \frac{n''(u)}{\sqrt{P_o}} \right] du \qquad (68)$$

$$+ \frac{d\phi(t)}{dt}$$

This is known as a second order loop.

The last operation is a frequency divider which results finally in the desired reference signal, r(t).

$$r(t) = \sqrt{2} \cos \left(2\pi f_o t + \theta(t) - \frac{e(t)}{2} \right) \qquad (69)$$

The error in the reference generated by the DPLL is thus found by solving for e(t). The solution techniques used to solve equations 24 and 25 are described in appendix C.

Multiplication and Integration

In the last section, solving for the coherent reference r(t) was described. Multiplying the incoming signal and integrating over the baud period, T, results in the statistic R.

$$R = 2\int_0^T M(t)\, E(t) \cos\,(2\pi f_o t + \theta(t))\, \cos\left(2\pi f_o t + \theta(t) - \frac{e(t)}{2}\right) dt \tag{70}$$

$$+ 2\int_0^T n(t)\, \cos\left(2\pi f_o t + \theta(t) - \frac{e(t)}{2}\right) dt$$

If $R > 0$, then the phase of $E(t)$ is taken as 0. If $R < 0$ then the assumed phase is π. The last integral on the right in equation 28 is a random zero mean Gaussian variable with variance NT. The decision process can be written as follows.

$$d + G(0) = R/(NT)^{1/2} \lesssim 0 \tag{71}$$

where $d = \int_0^T |E(t)| \cos\left[\frac{e(t)}{2}\right] dt/(NT)^{1/2}$

$G(0)$ is a Gaussian sample of unit variance. P_e, the bit error probability, is now easily found.

$$P_e = \text{erfc}\,(d) = \frac{1}{\sqrt{2\pi}} \int_d^\infty e^{-x^2/2}\, dx \tag{72}$$

The general method of analysis goes as follows. Using methods described in appendix A random ensembles of the input signals are generated and $\phi(t)$ is found for the sample. Next the appropriate loop equation is solved to get the phase error as a function of time. Lastly P_e is determined at appropriate sampling times and statistics on the error performance of the system are performed. Adequate statistics are insured by generating a sufficiently large number of sample signals.

This model provides an inexpensive simulation of all of the major aspects of the given BPSK demodulator including the effects of noise and nonlinearities in the PLL. The simulations required less than 8 minutes of CDC 6600 CPU time for each case.

SECTION V

PROPAGATION ENVIRONMENTS

Global morphology studies of scintillations at AFCRL (ref 18,19,20,21) indicate that scintillations are predominately equatorial and polar phenomena. The environments used in this study are intended to be representative of these two regions. The equatorial scintillations predominately occur within 15 degrees of the magnetic equator between 1900 and 0100 local time. They are present year around with maximums in frequency near the equinoxes. Some polar scintillation is virtually always present above 70 degrees geomagnetic latitude which is the scintillation boundary at about 0900 local time. The boundary moves south with time reaching about 57 degrees geomagnetic latitude at 2100 hours. The boundary is generally less than 60 degrees between 1800 and 2400 hours local. During disturbed magnetic conditions the scintillation boundaries can go further south. The severity of scintillations is not uniform in the polar region. The most severe occurances occur during the late evening hours in a region bounded on the south by the already mentioned boundary and extending northward 5 to 10 degrees.

In section II, the environmental description necessary to do the propagation section included the following parameters.

$\overline{n_e(X)}$ = mean electron density

$\overline{(n_e(X)^2} - \overline{n_e(X)}^2 / \overline{n_e(X)}^2 = \sigma_n^2$ = relative fluctuation power

ℓ_o = outer scale size

The mean electron density and the relative fluctuation power (RFP) are treated as separate parameters primarily because the available in situ data are in terms of σ_n^2 and ℓ_o not including $\overline{n_e(X)}$.

As the available in situ data was examined it became clear that insufficient data existed to unambiguously specify the propagation environments. In the equatorial region, there are two sets of data available. The first set by Kelly and Mozer* is from rockets launched from Natal, Brazil, and contains the only F region peak data known to the author. From these data, estimates of σ_n^2/ℓ_o and ℓ_o can be made. The estimates of σ_n^2/ℓ_o are shown in table 1. The second set of equatorial data is from Dyson (ref 11) and is from 446 km, above the F region peak. Only a value for σ_n^2/ℓ_o can be estimated and it is also in table 1. More satellite and rocket in situ data exist but thus far it has not yet been reduced.

In the polar regions the data are from Sagalyn* and Dyson (ref. 11). These data unfortunately only include altitudes above about 700 km. For these data both ℓ_o and σ_n^2/ℓ_o can be estimated. As seen in figure 7, ℓ_o and α_n^2/ℓ_o are larger and smaller respectively than their lower altitude counterparts near the equator.

TABLE I. ENVIRONMENT PARAMETERS (EQUATORIAL)

	ℓ_o(Km)	$\sigma_n^2/\ell_o(km^{-1})$
Kelley	1.25	$.126 \leq \sigma_n^2/\ell_o \leq .66$
Dyson	> .45	.22

Two other pieces of data are necessary to do the propagation and the subsequent systems analysis. First an estimate of $\overline{n_e(X)}$, the mean electron density is needed. The ionospheric profiles used for the equatorial and polar cases are shown in figure 8. It is also necessary

*Private communication with M.C. Kelly and R. Sagalyn.

to have an estimate of the drift velocity of the ionospheric structure. Measurements by Lincoln Laboratories* and Paulson and Hopkins (ref 11) near the equator indicate that 150 $\pm$ 75 meters/second are reasonable estimates. These values are also typical for polar regions*.

In the present calculations, due to the paucity of data, σ_n^2/ℓ_o and ℓ_o are assumed constant for the entire bottom side of the ionosphere. This use of the constant single values for α_n^2/ℓ_o and ℓ_o may at first seem a poor representation of the ionospheric structure. There is reason to believe, however, that single values are not unreasonable. As already noted ℓ_o and σ_n^2/ℓ_o tend to be larger and smaller, respectively, at high latitudes and altitudes than the corresponding quantities at lower altitudes and latitudes. From general considerations of the gradient drift and other instabilities, the author believes that the differences in ℓ_o and σ_n^2/ℓ_o are primarily altitude related since both these quantities at saturation are a function of the ionospheric gradients giving rise to the instability (See Sleeper, ref 23). The steeper gradients appear to peak in the lower F region in the late evenings hours in both the polar and equatorial regions. The steep gradients are most likely a result of recombination bottom upward of the F region as the solar ionization decreases. (Note that no mention has been made to the mechanisms actually driving the instability. This is because the saturation of the instability is not dependent on the driving mechanism but only the initial gradients and the mean electron density). The increased RFP and the maximum electron density of the F region peak conspire to make this region dominant in the propagation effects. Thus using the environment parameters representative of the F region peak is reasonable. This postulated dominance of the F peak

in producing propagation effects has been questioned by some (ref 24) but all measurements of the height of the perturbing regions known to the author indicate an altitude of about 300 km or less. The presence of Fresnel filtering in much propagation data also argues against thick striated layers. Hopefully, existing in situ data for equatorial high altitudes and for the polar F region peak in the F layer irregularity zone will soon be reduced, and the F layer peak question can be resolved.

The use of the specified values of α_n^2/ℓ_o for the polar regions is of unknown validity. It is believed by the author that the numbers are reasonable for the polar case but not necessarily optimum because the detailed gradient structure in the polar ionosphere does vary significantly from that near the equator.

The actual determination of the values for σ_n^2/ℓ_o and ℓ_o used in the following relevations resulted from an iteration between reasonable values for σ_n^2/ℓ_o, $\overline{n_e(X)}$, and ℓ_o and between extensive propagation data taken by Paulson and Hopkins (ref 22,25,26) at selected times from 1970-1972 near the equator. They assumed that scintillation existed when the fades exceeded 6 dB with some regularity. Three types of data were used here. Cumulative amplitude distributions for 250 MHz, statistics on fade duration for 250 MHz, and the 1 to 99 percent points of some 2.3 gigahertz peak to peak data were used to estimate α_n^2/ℓ_o and ℓ_o assuming $\overline{n_e(X)}$ of figure 8. It should be noted that the value of σ_n^2 can be varied against $\overline{n_e(X)}$ without changing the net propagation effects. Thus there is some flexibility in picking these parameters. In addition the choice of 150 meters per second for the ionospheric drift velocity influenced the final numbers. The final numbers found that agree with the to be described propagation are

$$\delta_n^2/\ell_o = 8.6\% \text{ km}^{-1}$$

$$\ell_o = 0.44 \text{ km}$$

These numbers represent a considerably less severe propagation environment than that represented by the Kelley data. Considering the great variability of all the environment parameters in both time and space and the fact that the propagation data are averaged through and over different nights, this difference is probably not significant. By varying the ionospheric drift velocity, the mean ionospheric profile, and the regions of the ionosphere that are unstable, the values above can be varied over considerable ranges and still accurately reproduce the propagation data. All that can be said is that no gross inconsistency has been revealed in this analysis between the propagation and environment data. Additional data on the properties of the ionosphere must be accumulated before more can be said.

Figure 9 contains the fade duration statistic averaged over all of the Paulson and Hopkins data sets. The agreement is reasonable. With the given data, the 1-99 percent peak-to-peak amplitude numbers were 24 and 2.6 dB respectively for 250 MHz and 2.3 gigahertz, respectively, which, is reasonable agreement with Paulson and Hopkins. Figure 10 is a comparison of experimental and calculated cumulative amplitude data. Finally Paulson and Hopkins report a correlation of 0.6 for two frequencies near 250 MHz separated by 50 MHz. The calculated value was 0.7. Thus for the equatorial region a consistent and reasonable set of environmental descriptors has been found. The use of data from two widely spaced frequencies also adds confidence in using those numbers to calculate for other frequencies.

The problem of finding descriptors for the polar region was hindered by a lack of data either in situ or propagation. As already mentioned the in situ data are only from very high altitudes, well above the F region peak. The only multifrequency propagation data are from Pope and Fritz (ref 27). These data was taken at 137 and 1695 MHz by examining Automatic Gain Control (AGC) records for ITOS I and ESSA 9 satellite systems. The 137 MHz data are Rayleigh scattered agreeing with my calculations using the assumed parameters. The 1695 MHz data are of limited use here for several reasons. The most important is that the S band transmissions were made when propagation conditions were most favorable in terms of lack of scintillation. Thus these data are probably not representative of scintillated conditions. The use of the environmental descriptors from the equator in the polar regions is not inconsistent with these data, but that is all that can be said until additional data are available.

SECTION VI
SAMPLE RESULTS

To illustrate typical calculations, the performance of a Binary Frequency Shift Key (BFSK) and a Binary Phase Shift Key (BPSK) system were calculated in the polar and equatorial environments previously described. The scenarios are a synchronous satellite down to an aircraft going 300 m/sec at the equator and in the polar region beneath the north wall of th ionospheric trough. The frequency is 250 MHz. Figure 11 contains the calculated correlation functions of the signals. The equatorial case is a Rayleigh scattering case. The polar case is neither Rayleigh or Rician since the variance of the in phase and out phase components are not equal.

Both modems had a 200 Hz bandwidth and a bit period of 10^{-2} seconds. The loop bandwidth of the PSK receiver is 12 hertz (a=16, K=32). Figures 12 and 13 contain the results of the link calculations. Shown are the signal to noise ratios necessary for a 10^{-4} bit error rate, the bit error rates for all the cases, the maximum error free transmission time over the total simulation time, and the window statistics. The meaning of the window statistics can be interpreted as follows. For the FSK, polar, and 15 dB calculation, the point at ΔT=5 seconds means that in a minute there will be three intervals of 5 seconds or greater with no bit errors.

At 15 dB the PSK link is superior, but this trend is reversed at 25 dB. This is contrary to the results using a linear analysis of the PSK receiver illustrating the necessity of treating the nonlinearities of the PSK receiver with noise. A valuable lesson to be learned from

these simple results is that even though the bit error probabilities are relatively large, significant information could be transmitted provided the message is appropriately structured. At present various schemes are being considered. One possible way is to interleave the bit stream over a suitable interval and use coding. Another method for simple messages is to use an algorithm which constructs a message out of correctly received segments. The results of this work is in terms of message reception probabilities. Message reception probabilities are ultimately the most desired result and the algorithms to calculate these results are being constructed.

SECTION VII

SUMMARY

This report has demonstrated methods to calculate message reception probabilities and other useful information starting from the statistical description of the propagation environment. A discussion on the state of knowledge of the ambient environments is also given. The presented methods provide sufficient accuracy to examine the various questions affecting the satellite communications systems mentioned in the introduction.

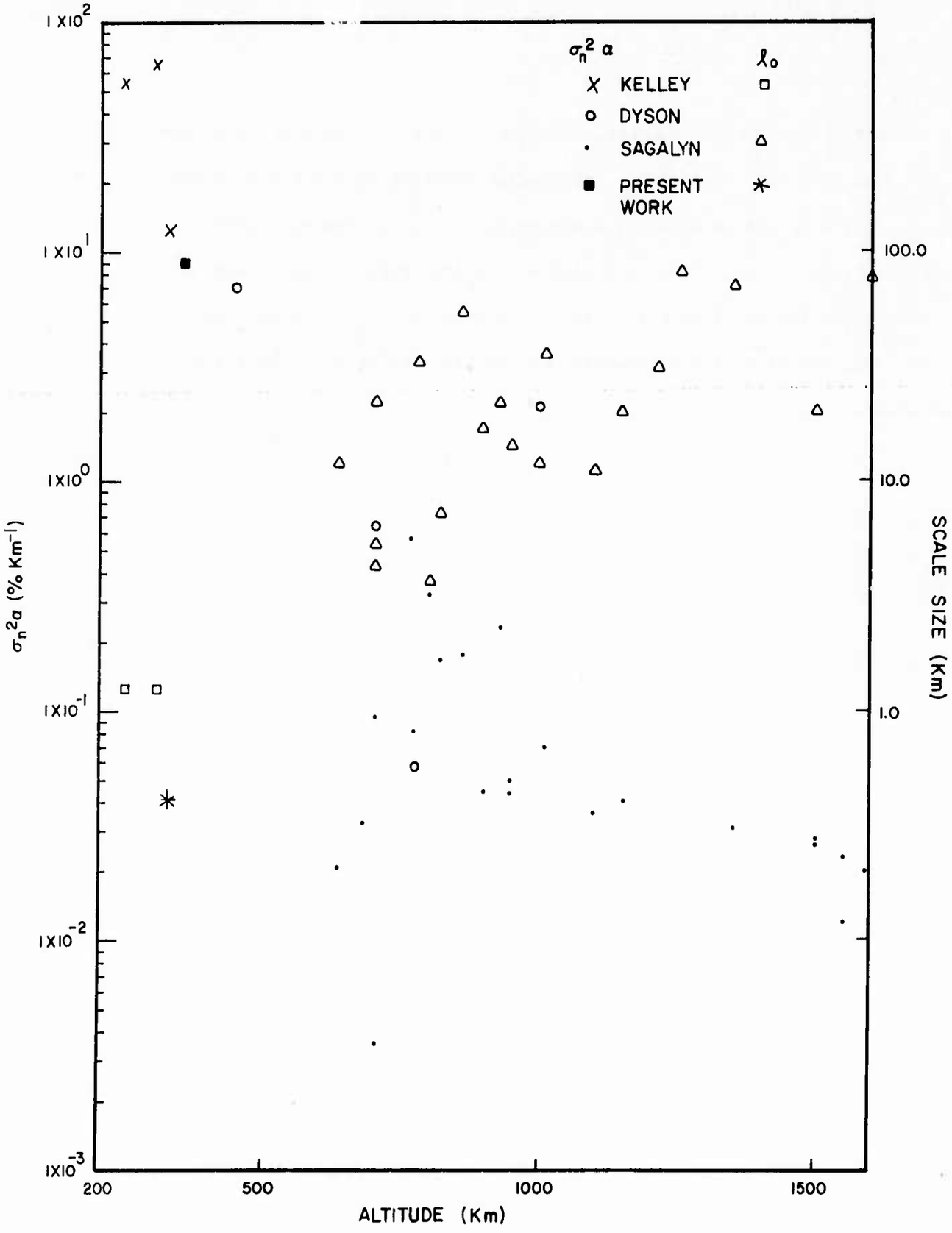

Figure 7. Ionospheric Parameters

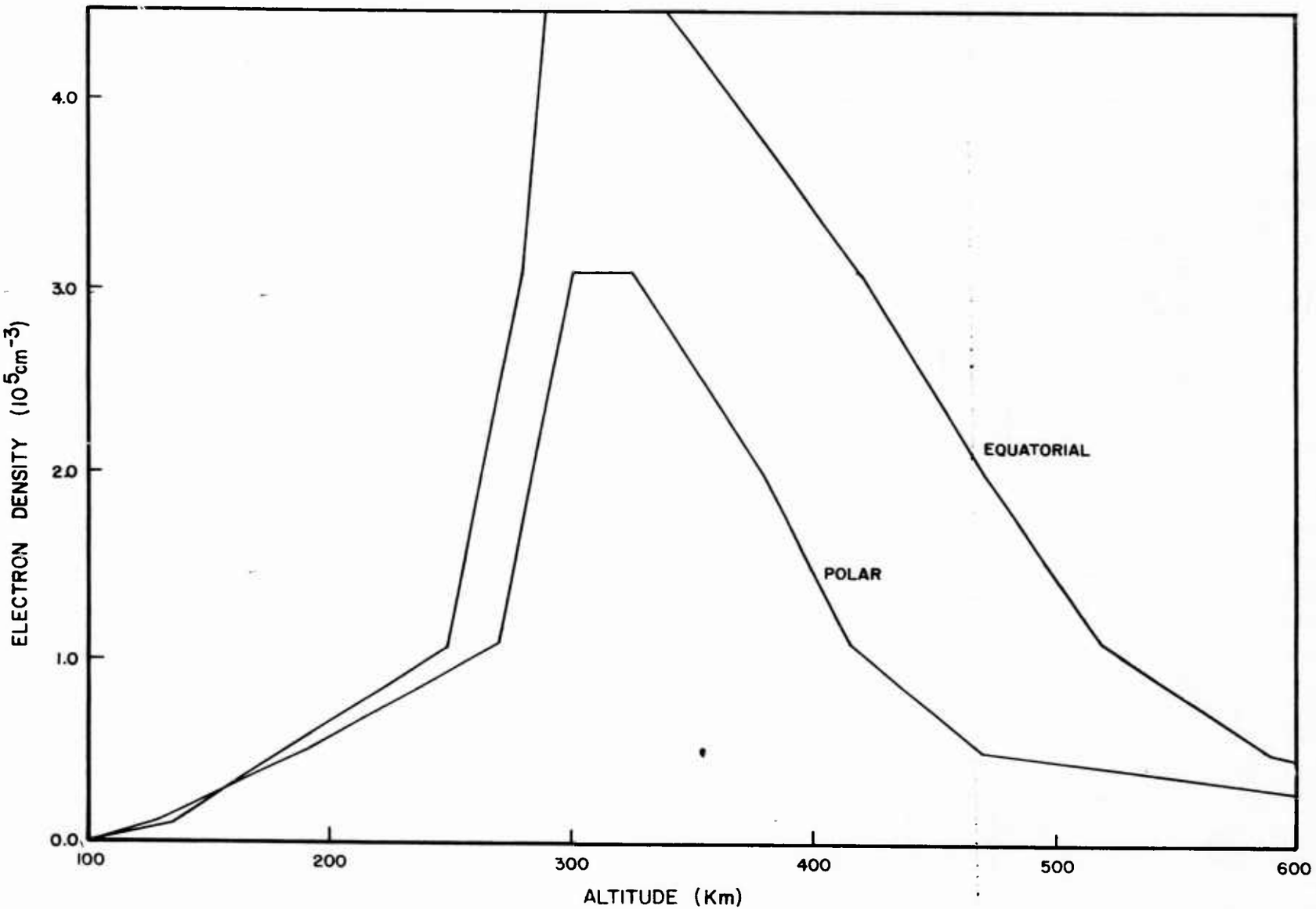

Figure 8. Model Ionospheres

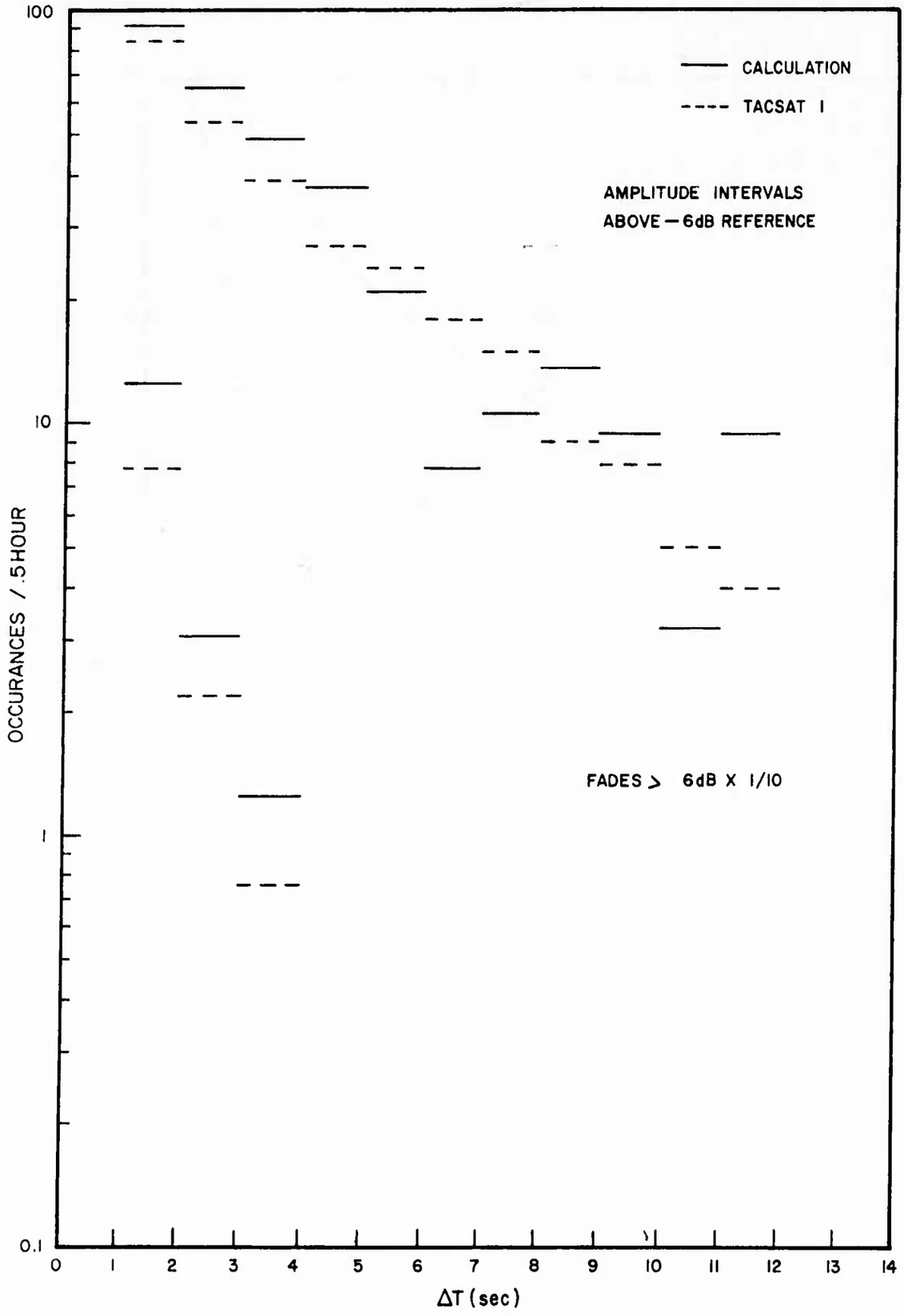

Figure 9. Fade Statistics

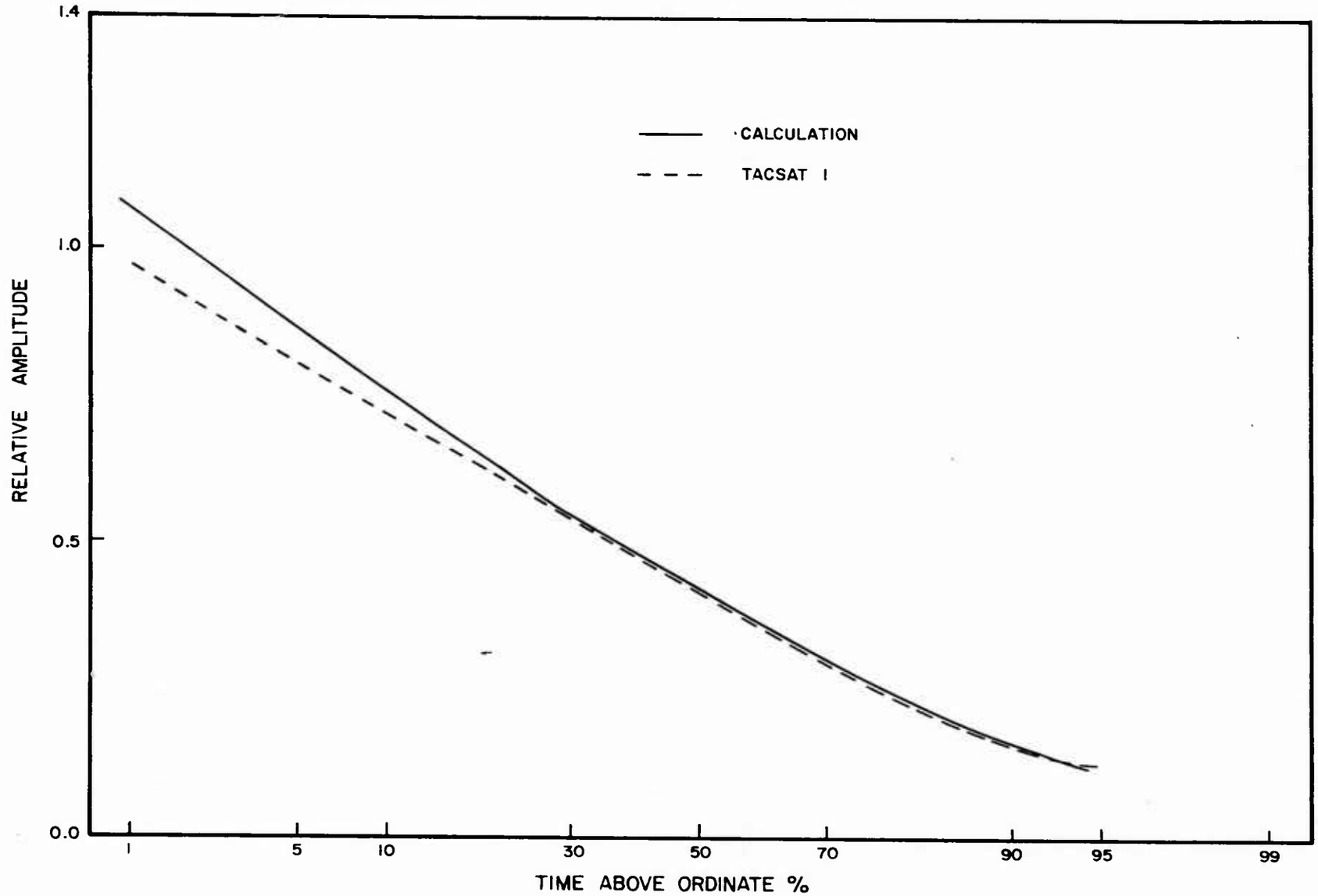

Figure 10. Cumulative Amplitude Distributions

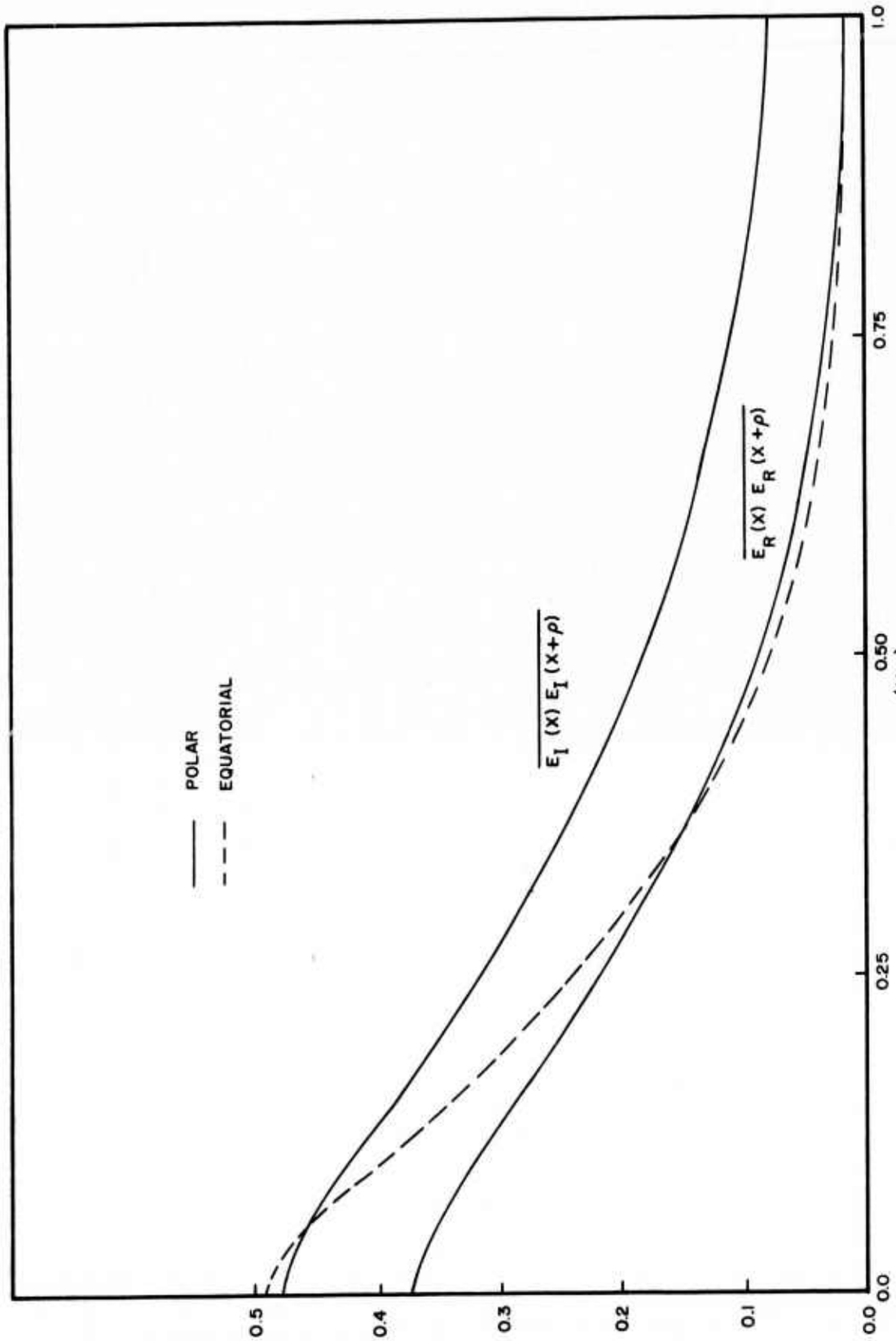

Figure 11. Signal Correlation Functions

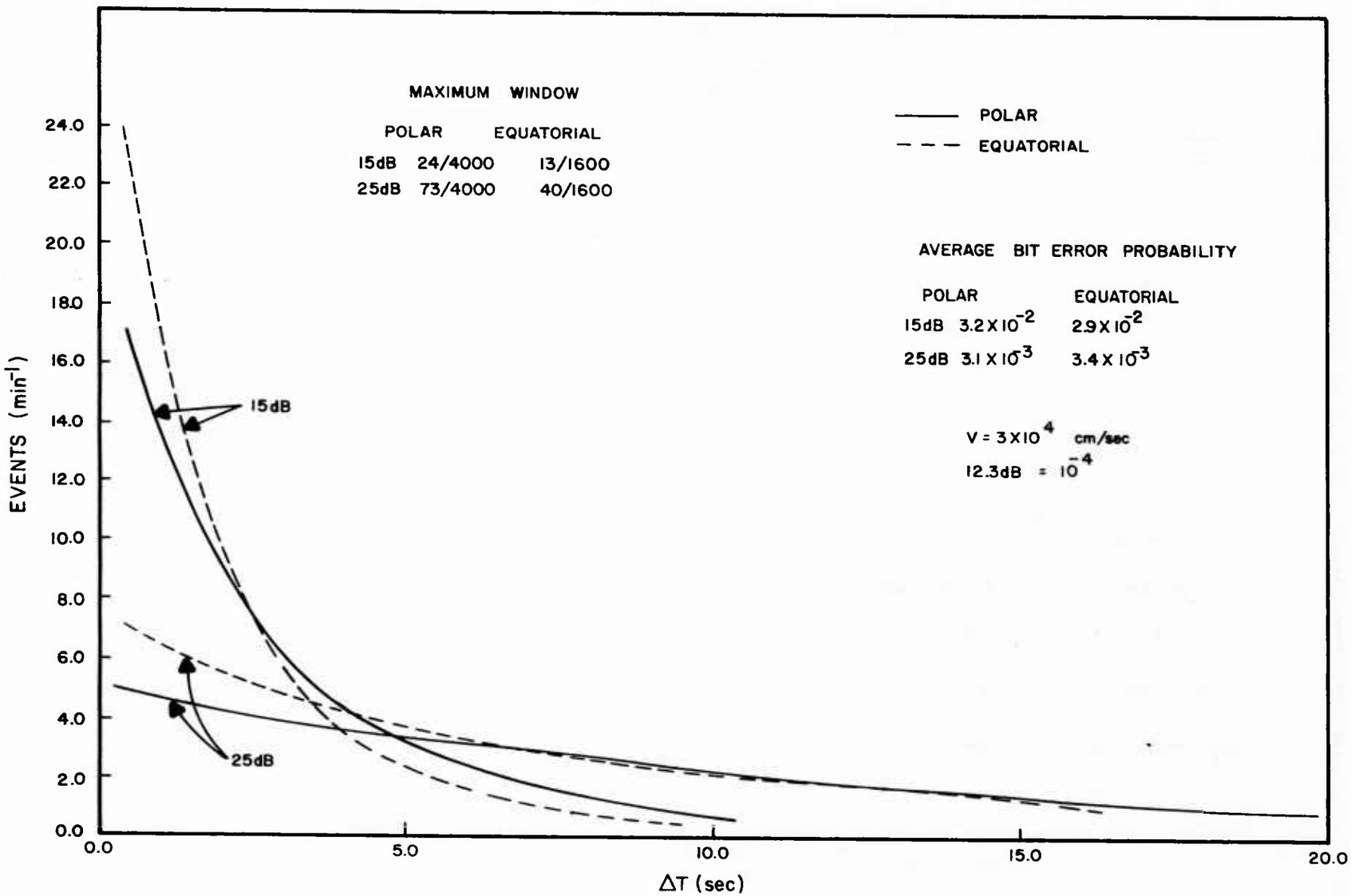

Figure 12. FSK Link Performance

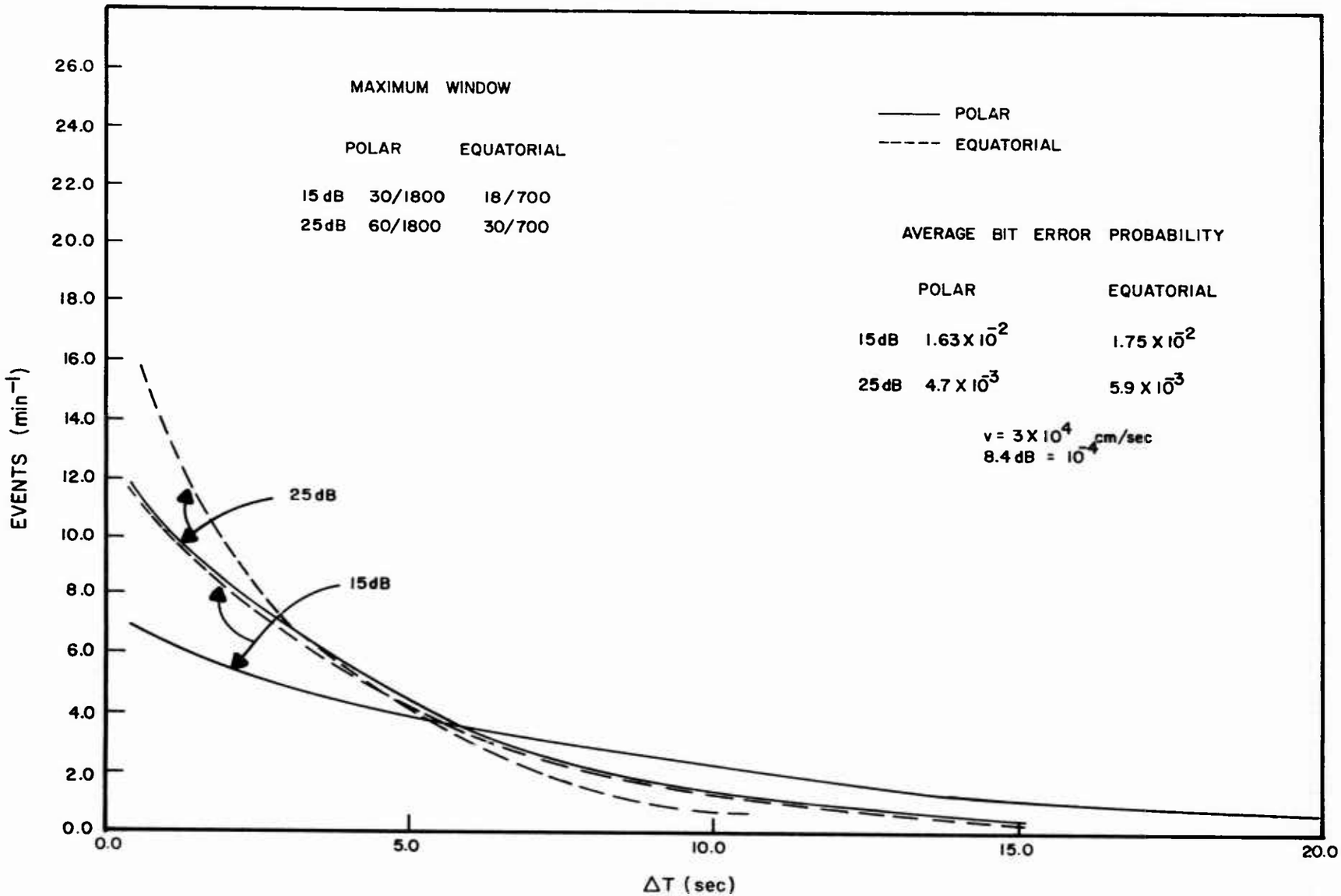

Figure 13. PSK Link Performance

Appendix A

Generation of Complex Correlated Random Sequences

Let f(t) be a zero mean random Gaussian variable on the domain (-T,T). f(t) can be expanded in a Fourier series.

$$f(t) = \frac{1}{2}\sum_{n=-\infty}^{\infty} C_n \, \ell^{i\omega_n t}, \quad \omega_n = \frac{n\pi}{T} \tag{A1}$$

$$C_n = \frac{1}{T}\int_{-T}^{T} f(t) \, \ell^{-i\omega_n t} \, dt \tag{A2}$$

Let $$G(t-t') = \overline{f^*(t)f(t')} \tag{A3}$$

$$F(t-t') = \overline{f(t)f(t')} \tag{A4}$$

Then $$\lim_{T\to\infty}(T\overline{C_n^* \, C_m}) = 0, \quad m \neq n, \quad m \neq 0 \tag{A5}$$

$$\lim_{T\to\infty}(T\overline{C_m^* \, C_m}) = 4\int_0^{2T} d\alpha \, G(\alpha) \cos(\alpha\omega_m) \tag{A6}$$

$$= T \, K_m$$

$$\lim_{T\to\infty}(T\overline{C_n \, C_m}) = 0, \quad m \neq n, \quad m \neq 0$$

$$\lim_{T\to\infty}(T\overline{C_m \, C_{-m}}) = 4\int_0^{2T} d\alpha \, F(\alpha) \cos(\alpha\omega_m) \tag{A7}$$

$$= T(L_m + i \, M_m) \tag{A8}$$

If T is chosen such that $F(t) = G(t) \approx 0$ for $t \geq T$, the limits in equations A5, A6, A7, and A8 can be assumed. Now if $C_m = C_{mr} + iC_{mi}$, and using equations A5, A6, A7 and A8, then with $m \neq 0$.

$$\overline{C_{mr}\, C_{mr}} = \overline{C_{mi}\, C_{mi}} = K_m/2 \tag{A9}$$

$$\overline{C_{mr}\, C_{mi}} = 0 \tag{A10}$$

$$\overline{C_{mr}\, C_{-mr}} = \overline{-C_{mi}\, C_{-mi}} = L_m/2 \tag{A11}$$

$$\overline{C_{mr}\, C_{-mi}} = \overline{C_{-mr}\, C_{mi}} = M_m/2 \tag{A12}$$

Since C_{mr}, C_{mi}, C_{-mr}, and C_{-mi} are random Gaussian variables, the joint probability distribution function of these variables can be written in terms of K_m, L_m, and M_m.

$$P(C_{mr},C_{mi},C_{-mr},C_{-mi}) = C \exp$$

$$\left\{\left[\left|C_{mr}\ C_{mi}\ C_{-mr}\ C_{-mi}\right| \begin{vmatrix} K_m & 0 & -L_m & -M_m \\ 0 & K_m & -M_m & L_m \\ -L_m & -M_m & K_m & 0 \\ -M_m & L_m & 0 & K_m \end{vmatrix} \begin{vmatrix} C_{mr} \\ C_{mi} \\ C_{-mr} \\ C_{-mi} \end{vmatrix}\right] \Big/ (K_m^2 - L_m^2 - M_m^2)\right\} \tag{A13}$$

This expression can be simplified by diagonalizing the 4 x 4 matrix. To diagonalize the above matrix, a transformation matrix must be found with the following properties.

$$T^{-1}T = TT^{-1} = I \tag{A14}$$

$$T\,Q\,T^{-1} = R \tag{A15}$$

where I is the identity matrix, Q is the 4 x 4 matrix in equation 13, and R is a diagonal matrix with diagonal elements λ_1, λ_2, λ_3, and λ_4. The diagonal elements are easily solved for.

$$\lambda_1 = \lambda_2 = K_m + \sqrt{L_m^2 + M_m^2} \tag{A16}$$

$$\lambda_3 = \lambda_4 = K_m - \sqrt{L_m^2 + M_m^2} \tag{A17}$$

A matrix T, with the desired properties is

$$T = \frac{1}{\sqrt{2}} \begin{vmatrix} 1 & 0 & L_m/\sqrt{} & M_m/\sqrt{} \\ 0 & 1 & M_m/\sqrt{} & -L_m\sqrt{} \\ -L_m/\sqrt{} & -M_m/\sqrt{} & 1 & 0 \\ -M_m/\sqrt{} & L_m/\sqrt{} & 0 & 1 \end{vmatrix} \tag{A18}$$

where $\sqrt{} = \sqrt{L_m^2 + M_m^2}$. The probability density function can now be written as

$$P(C_{m_r}', C_{m_i}', C_{-mr}', C_{-mi}') = C' \exp\left\{ -\frac{1}{2}\left[\frac{2(C_{mr}'^2 + C_{mi}'^2)}{K_m + \sqrt{L_m^2 + M_m^2}} + \frac{2(C_{-mr}'^2 + C_{-mi}'^2)}{K_m - \sqrt{L_m^2 + M_m^2}} \right] \right\} \tag{A19}$$

where

$$\begin{vmatrix} C_{mr} \\ C_{mi} \\ C_{-mr} \\ C_{-mi} \end{vmatrix} = \frac{1}{\sqrt{2}} \begin{vmatrix} 1 & 0 & -L_m/\sqrt{} & -M_m/\sqrt{} \\ 0 & 1 & -M_m/\sqrt{} & L_m/\sqrt{} \\ L_m/\sqrt{} & M_m/\sqrt{} & 1 & 0 \\ M_m/\sqrt{} & -L_m/\sqrt{} & 0 & 1 \end{vmatrix} \begin{vmatrix} C'_{mr} \\ C'_{mi} \\ C'_{-mr} \\ C'_{-mi} \end{vmatrix} \tag{A20}$$

The primed variables are also random Gaussian variables with variances as shown in equation A19. Generating a simple of f(t) on the interval $-T \leq t \leq T$ is now straight forward. For each $m \neq 0$, sample a Gaussian distribution four times to get values of C'_{mr}, C'_{mi}, C'_{-mr}, and C'_{-mi}, transform using equation 20 to unprimed variables, and form the random Fourier coefficient by $C_m = C_{mr} + iC_{mi}$. For m = 0, another procedure must be used. From equations A6 and A8

$$\overline{C_{or}^2} + \overline{C_{oi}^2} = K_o \tag{A21}$$

$$\overline{C_{or}^2} - \overline{C_{oi}^2} = L_o \tag{A22}$$

$$\overline{C_{or}\, C_{oi}} = M_o/2 \tag{A23}$$

Thus

$$\overline{C_{or}^2} = (K_o + L_o)/2 \tag{A24}$$

$$\overline{C_{oi}^2} = (K_o - L_o)/2 \tag{A25}$$

The joint probability function can now be written as

$$P(C_{or}, C_{oi}) = C \exp \left\{ \left[\left| C_{oi} \; C_{or} \right| \right. \right.$$

$$\left. \left. \begin{vmatrix} (K_o - L_o) & -M_o \\ -M_o & (K_o + L_o) \end{vmatrix} \begin{vmatrix} C_{oi} \\ C_{or} \end{vmatrix} \Big/ (K_o^2 - L_o^2 - M_o^2) \right] \right\} \tag{26}$$

Following the same procedure as with $m \neq 0$, the probability matrix can be diagonalized.

Let

$$C_{or} = [(K_o + L_o)/2]^{1/2} \; (C'_{or} + C'_{oi}) \tag{A27}$$

$$C_{oi} = [(K_o - L_o)/2]^{1/2} \; (C'_{or} - C'_{oi}) \tag{A28}$$

Then

$$P(C'_{or}, C'_{oi}) = C \exp \left\{ -\frac{1}{2} \left[\frac{2\left(K_o^2 - L_o^2 - M_o \left(K_o^2 - L_o^2\right)^{1/2}\right)}{K_o^2 - L_o^2 - M_o^2} \; C'^{\,2}_{or} \right. \right.$$

$$\left. \left. + \frac{2(K_o^2 - L_o^2 + M_o \left(K_o^2 - L_o^2\right)^{1/2})}{K_o^2 - L_o^2 - M_o^2} \; C'^{\,2}_{oi} \right] \right\} \tag{A29}$$

$$= C \exp \left\{ -\frac{1}{2} \left[C'^{2}_{or}/\sigma_r^2 + C'^{2}_{oi}/\sigma_i^2 \right] \right\} \tag{A30}$$

To generate C_{or} and C_{oi}, a random Gaussian sample of C'_{or} and C'_{oi} are generated with the variances σ_r^2 and σ_i^2 respectively and used in equations A27 and A28. After the random complex Fourier coefficients

are found for all m, the sample f(t) is calculated by inverse Fourier transforming as in equation A1.

Appendix B

Noise Derived Power Spectral Density of a Square Law Device

Let $$Y(t) = a(s(t) + n(t))^2 \tag{B1}$$

where s(t) and n(t) are the signal and noise input respectively to the square law device.

$$Y(t) = a[s^2(t) + 2n(t)s(t) + n^2(t)] \tag{B2}$$

If n(t) is a zero mean, stationary, gaussian process and independent of s(t) and if s(t) is stationary, then

$$\overline{Y} = a[\overline{s^2} + \overline{n^2}] \tag{B3}$$

Also

$$\overline{Y^2} = a^2[\overline{s^4} + 6\ \overline{s^2}\ \overline{n^2} + \overline{n^4}] \tag{B4}$$

The autocorrelation function of Y(t) is

$$R_y(\tau) = a^2[(s(t) + n(t))^2(s(t + \tau) + n(t + \tau))^2] \tag{B5}$$

$$= a^2[\overline{s^2(t)s^2(t + \tau)} + \overline{n^2(t)n^2(t + \tau)}$$

$$+ 4\ \overline{s(t)s(t + \tau)}\ \overline{n(t)n(t + \tau)} + 2\ \overline{s^2(t)}\ \overline{n^2(t)}] \tag{B6}$$

$$R_y(\tau) = a^2[R_s2(\tau) + 2\,\overline{s^2}\,\overline{n^2} + 4\,R_s(\tau)R_n(\tau) + R_n2(\tau)] \tag{B7}$$

The last three terms in equation B7 are noise derived. The power spectral density of Y(t) is the Fourier transform of $R_y(\tau)$. The spectral density associated with the middle terms is

$$S_{sxn}(f) = 4a^2 \int_{-\infty}^{\infty} R_s(\tau)\, R_n(\tau) e^{-i2\pi f\tau}\, d\tau$$

$$+ 2a^2\,\overline{s^2}\,\overline{n^2}\,\delta(f) \tag{B8}$$

$$= 4a^2 \int_{-\infty}^{\infty} S_n(f')\, S_s(f-f')\, df'$$

$$+ 2a^2\,\overline{s^2}\,\overline{n^2}\,\delta(f) \tag{B9}$$

Since n(t) is Gaussian,

$$a^2R_n2(\tau) = 2a^2 R_n^2(\tau) + a^2\,\overline{s^2}^2 \tag{B10}$$

Thus the spectral density of the last term is

$$S_{nxn}(f) = 2a^2 \int_{-\infty}^{\infty} S_n(f')\, S_n(f-f')\, df' \tag{B11}$$

$$+ a^2\,\overline{s^2}^2\,\delta(f)$$

The total power spectral density from noise related terms for the square law device is

$$S_{sxn}(f) + S_{nxn}(f) = 4a^2\, S_n(f) * S_s(f)$$

$$+ 2a^2 S_n(f) * S_n(f) + [\overline{s^2}^2 + \overline{s^2}\,\overline{n^2}]a^2\delta(f) \tag{B12}$$

where * denotes a convolution operation. It is important to note that the process with a spectral density of $S_n(f) * S_n(f)$ is not gaussian as is the $S_n(f) * S_s(f)$ process.

Appendix C

SOLUTION TECHNIQUES FOR THE FIRST AND SECOND ORDER LOOP ERROR EQUATIONS

The equation for the second order loop equation to be solved is

$$\frac{de(t)}{dt} = \frac{d\theta(t)}{dt} - K\sqrt{\frac{P(t)}{P_o}}\sin(e(t)) - \frac{K}{\sqrt{P_o}}n(t)$$

$$- aK\int_o^t\left[\sqrt{\frac{P(u)}{P_o}}\sin(e(u)) + \frac{n(u)}{\sqrt{P_o}}\right]du \qquad (C1)$$

where n(t) is a zero mean Gaussian process with a power spectral density of N/2 centered at f = 0. Let

$$F(t) = -aK\int_o^t\left[\sqrt{\frac{P(u)}{P_o}}\sin(e(u)) + \frac{n(u)}{\sqrt{P_o}}\right]du \qquad (C2)$$

Then

$$F(t+\Delta t) \approx F(t) - aK\sqrt{\frac{P(t)}{P_o}}\sin(e(t))\Delta t - \frac{aK}{\sqrt{P_o}}I_1(t+\Delta t)\Delta t^{1/2} \qquad (C3)$$

where $I_1(t+\Delta t)\,t^{1/2} = \int_t^{t+\Delta t} n(u)du$.

Equation 1 can be similarly integrated for a result for e(t+Δt) where it is assumed that Δt is sufficiently small so that P(t) and sin(e(t)) do not change significantly over Δt.

$$e(t+\Delta t) = e(t) + \left[\frac{d\theta(t)}{dt} - K\sqrt{\frac{P(t)}{P_o}}\sin(e(t)) + F(t)\right]\Delta t$$

$$- \frac{aK}{2}\sqrt{\frac{P(t)}{P_o}}\sin(e(t))\Delta t^2 - \frac{aK}{\sqrt{P_o}}I_2(t+\Delta t)\Delta t^{3/2} - \frac{K}{\sqrt{P_o}}I_1(t+\Delta t)\Delta t^{1/2} \qquad (C4)$$

where

$$I_2(t+\Delta t)\Delta t^{3/2} = \int_o^{\Delta t} du \int_t^{t+u} n(v)dv$$

If $\Delta t > 1/W$ then the following relations hold

$$\overline{I_2(0)\ I_2(n\Delta t)} = \delta(n)\ \frac{N}{4} \tag{C5}$$

$$\overline{I_2(0)\ I_1(n\Delta t)} = \delta(n)\ \frac{N}{4} \tag{C6}$$

$$\overline{I_1(0)\ I_1(n\Delta t)} = \delta(n)\ \frac{N}{2} \tag{C7}$$

Since the noise is assumed a Gaussian process, the noise integrals can be expressed as

$$I_1(\Delta t) = \sqrt{\frac{N}{2}}\left[0.923\ G_1(0) + 0.383\ G_2(0)\right] \tag{C8}$$

$$I_2(\Delta t) = \sqrt{\frac{N}{4}}\left[0.923\ G_1(0) - 0.383\ G_2(0)\right] \tag{C9}$$

In order to solve equation C1, both F(t) and e(t) must be updated every time step. The equation for F(t+Δt) can be written

$$F(t+\Delta t) = F(t) + (b_1\Delta t^{\frac{1}{2}} + b_2)\Delta t^{\frac{1}{2}} \tag{C10}$$

where

$$b_1 = -.\ aK\sqrt{\frac{P(t)}{P_o}}\ \sin\left[e(t)\right] = ac_1 \tag{C11}$$

$$b_2 = -\frac{aK}{\sqrt{P_o}}\ I_1(t+\Delta t) = ac_2 \tag{C12}$$

For $e(t+\Delta t)$

$$e(t+\Delta t) = e(t) + \left\{\left[(a_1\Delta t^{\frac{1}{2}} + a_2)\Delta t^{\frac{1}{2}} + a_3\right]\Delta t^{\frac{1}{2}} + a_4\right\}\Delta t^{\frac{1}{2}} \tag{C13}$$

where
$$a_1 = b_1/2 \tag{C14}$$

$$a_2 = -\frac{aK}{\sqrt{P_o}} I_2(t+\Delta t) \tag{C15}$$

$$a_3 = \frac{d\theta(t)}{dt} + F(t) + c_1 \tag{C16}$$

$$a_4 = c_2 \tag{C17}$$

The overall solution method is now a straightforward procedure. First the initial conditions are:

$$F(0) = 0 \tag{C18}$$

$$e(0) = 0 \tag{C19}$$

Next pick an initial Δt. Then proceed through the following.

1. Calculate b_1 and b_2.
2. Solve equation B10
3. Calculate a_1, a_2, a_3, and a_4.
4. Solve equation B13

5. Check size of time step.

If $|e(t+\Delta t) - e(t)| > 20°$, then $\Delta t = 3\Delta t/4$ and

If $|e(t+\Delta t) - e(t)| < 5°$, then $\Delta t = 4\Delta t/3$, increment total time, and go to step 1.

The method of solution outlined, while somewhat inelegant, does provide a reasonable simulation of the nonlinear phase lock loop behavior in the presence of noise while remaining simple and efficient on a digital computer.

The method of solution of the first order loop is the same as for the second order loop with $a = 0$.

REFERENCES

1. Rino, C.L. and Fremouw, E.J., "Statistics for Ionospherically Diffracted VHF/UHF Signals," Radio Sci., Vol. 8, No. 3, pp. 223-233, (1973).

2. Fremouw, E.J., Rino, C.L. and Long, R.A., (This reference is available to qualified military or government requestors from AFWL/DYT).

3. Sachs, D.L., (This reference is available to qualified military or government requestors from AFWL/DYT).

4. Hendrick, R.W. and Shaeffer, L., Propagation in Striated Media, MRC-R-118, Mission Research Corporation, Apr 1974 (to be published).

5. Bowhill, S.A., "Statistics of a Radio Wave Diffracted by a Random Ionosphere," Journal of Research of NBS - D. Radio Propagation, Vol. 65D, No. 3, May-June 1961.

6. Briggs, B.H. and Parkin, I.A., "On the Variation of Radio Star and Satellite Scintillations with Zenith Angle," Journal of Atmospheric and Terrestrial Physics, Vol. 25 (1963).

7. Evans, J.V. (Editor), Millstone Hill Radar Propagation Study: Scientific Results - Part II, Lincoln Laboratory Technical Report 509, 13 Nov 1973.

8. Crane, R.K., "Spectra of Amplitude and Phase Scintillation," to appear in the Proceedings of the 1975 Symposium on the Effect of the Ionosphere on Space Systems and Communication, 20-22 Jan 75.

9. Uscinski, B.J., " The Multiple Scattering of Waves in Irregular Media," Phil. Trans., Royal Society of London, Vol. 262, p. 609 (1968).

10. Tatarskii, V.I., The Effects of the Turbulent Atmosphere on Wave Propagation, National Science Foundation TT-68-50464 (1971).

11. Dyson, P.L., McClure, J.P. and Hanson, W.B., "In Situ Measurements of the Spectral Characteristics of F Region Ionospheric Irregularities," Journal of Geophysical Research, Vol. 79, Apr 1, 1974.

12. Rhino, C.L., "Some Unique Features of the Transionospheric Channel", to appear in the Proceedings of the 1975 Symposium on the Effect of the Ionosphere on Space Systems and Communications, 20-22 Jan 75.

13. Liu, C.H., Wernick, A.W. and Yeh, K.C., "Propagation of Pulse Trains Through a Ransom Medium," IEEE Transactions on Antennas and Propagation, Jul 74.

14. Ulaszek, S.J., Liu, C.H. and Yeh, K.C., "Frequency Correlation and Coherent Bandwith of Transionosphereic Signals," to appear in the Proceedings of the 1975 Symposium on the Effect of the Ionosphere on Space Systems and Communications, 20-22 Jan 75.

15. Helstrom, C.W., Statistical Theory of Signal Detection, Pergamon Press Inc., N.Y., 1968.

16. Roberts, J., Mower, V., Marshall, J., Hennings, R. and Watson, D., PSK Satellite Communications Systems in a Nuclear Environment (U), DNA 3289, 26 Oct 73.

17. Van Trees, H.L., Detection Estimation, and Modulation Theory, John Wiley and Sons, Inc., New York, 1971.

18. Aarons, J.H., Whitney, H.E. and Allen, R.S., "Global Morphology of Ionospheric Scintillations", Proc. IEEE, Vol. 59, 1971.

19. Aarons, J.H., "High Latitude Morphology of Ionospheric Scintillations," to appear in the Proceedings of the 1975 Symposium on the Effect of the Ionosphere on Space Systems and Communications, 20-22 Jan 75.

20. Sagalyn, R.C., Smiddy, M. and Ahmend, M., "High-Latitude Irregularities in the Top Side Ionosphere Based on IsisI Thermal Ion Probe Data", Journal Geophysical Research, Vol. 79, 1974.

21. Fremouw, E.J.,and Rhino, C.L., "An Empirical Model for Average F-Layer Scintillation at VHF/UHF," Radio Sci., Vol. 8, 1973.

22. Paulson, M.R. and Hopkins, R.V.F., Effects of Equatorial Scintillation Fading on SATCOM Signals, Naval Electronics Laboratory Center TR 1875, 8 May 73.

23. Sleeper, A.M. and Weinstock, J. "Nonlinear Theory of Density Flucuations in Turbulent Plasmas," Phys. of Fluids, Vol. 15, Aug 71.

24. Booker, H.G., "The Role of the Magnetosphere in Satellite and Radio-Star Scintillations" to appear in the Proceedings of the 1975 Symposium on the Effect of the Ionosphere on Space Systems and Communications, 20-22 Jan 75.

25. Paulson, M.R., Some Amplitude Duration Distributions for Equatorial Scintillation of TACSAT I UHF Signals, Naval Electronics Laboratory Center TR 2502, 4 Oct 73.

26. Paulson, M.R. and Tyner, An Investigation of Equatorial Fading of TACSAT I UHF Signals, Naval Electronics Laboratory Center TN 1837, 14 Apr 71.

27. Pope, J.H. and Fritz, R.B., "High Latitude Scintillation Effects on Very High Frequency (VHF) and S-Band Satellite Transmission," Indian J. of Pure and Applied Physics, Vol. 9, Aug 1971.